REPORT DOCUMENTATION PAGE

AFOSR-TR-96

0352

1. AGENCY USE ONLY (Leave blank)	2. REPORT DATE	3. REPORT TYPE AND DATES COVERED
	6/30/96	Final Report 11/01/91 - 04/30/96

4. TITLE AND SUBTITLE
Optoelectronics Generation and Detection of Intense Terahertz Electromagnetic Pulses

5. FUNDING NUMBERS
~~F49620-92-J-0036~~
2301/AS
61102F

6. AUTHOR(S)
T. Heinz, et al.

7. PERFORMING ORGANIZATION NAME(S) AND ADDRESS(ES)
Columbia University
Columbia Radiation Laboratory
530 West 120th St. Room 1001, MC8903
New York, NY 10027

8. PERFORMING ORGANIZATION REPORT NUMBER
~~F49620-92-J-0036~~

9. SPONSORING/MONITORING AGENCY NAME(S) AND ADDRESS(ES)
AFOSR/NE
110 Duncan Avenue Suite B115
Bolling AFB DC 20332-0001

10. SPONSORING/MONITORING AGENCY REPORT NUMBER
F49620-92-J-0036

11. SUPPLEMENTARY NOTES
The view, opinions and/or findings contained in this report are those of the author(s) and should not be construed as an official Department of the Army position, policy, or decision, unless so designated by other documentation.

12a. DISTRIBUTION/AVAILABILITY STATEMENT
Approved for public release; distribution unlimited.

12b. DISTRIBUTION CODE

19960726 050

13. ABSTRACT *(Maximum 200 words)*

In studies supported by this research contract, we have investigated both the fundamental aspects and spectroscopic applications of optoelectronic techniques of generation and detection of subpicosecond electromagnetic pulses. The original research objectives pursued under this contract included the development of significant new capabilities and an improved fundamental understanding of the physical mechanisms involved in the optoelectronic generation and detection of THz radiation. The characteristics of such optically excited THz emitters with respect to the scaling of their peak THz intensities using higher optical fluences and enhancements in their THz frequency response were also to be explored. One of the main issues addressed by these studies was the development of new bright coherent sources and sensitive detectors to enable linear and nonlinear spectroscopy in the far-infrared region of the electromagnetic spectrum.

14. SUBJECT TERMS			15. NUMBER OF PAGES 54
			16. PRICE CODE
17. SECURITY CLASSIFICATION OF REPORT	18. SECURITY CLASSIFICATION OF THIS PAGE	19. SECURITY CLASSIFICATION OF ABSTRACT	20. LIMITATION OF ABSTRACT
UNCLASSIFIED	UNCLASSIFIED	UNCLASSIFIED	UL

Optoelectronic Generation and Detection of Intense Terahertz Electromagnetic Pulses.

Principal Investigator: Tony F. Heinz

Departments of Electrical Engineering and Physics

Columbia University

500 West 120th Street

New York, New York 10027

Final Technical Report

November 1, 1991 - April 30, 1996

Grant #F49620-92-J-0036

Submitted to H. Schlossberg

Air Force Office of Scientific Research

Building 410

Bolling Air Force Base, DC 20332-6448

Table of Contents.

I. Introduction 1

II. Key Accomplishments 1

III. Optoelectronic Generation of THz radiation from semiconductor devices 3

A. THz radiation from large-aperture Si p-i-n diodes 3
B. Study of carrier dynamics in semiconductors using optically induced THz radiation 9
1. THz radiation induced by sub-band gap femtosecond optical excitation of semiconductor surfaces 9
2. Transient velocity overshoot effects observed in THz radiation from GaAs p-i-n diodes 15
C. Study of the physical mechanism of THz generation in bulk GaAs 19
D. Observation of Gunn Oscillation by triggering a vertical Gunn diode with femtosecond optical pulses 25

IV. Tunable narrowband THz radiation 26

A. Chirped pulse beating 27
1. Optical cross-correlation measurements 30
B. A tunable THz beam system using photoconducting dipole antennas 31
C. Tunable THz detection 33
D. Generation of intense tunable THz from photoconducting antennas 34
E. Tunable THz radiation by difference-frequency generation in $LiNbO_3$ 35

V. Ultra-broadband THz radiation 36

A. Generation of THz radiation from poled polymers 37
B. Coherent detection of free space THz radiation by electro-optic sampling 40
C. Ultra-broadband coherent THz spectroscopy using optical rectification and electro-optic sampling 43

VI. Optoelectronic detection of transient electric fields in high-speed circuits 45

A. High-Speed electrical sampling using optical second-harmonic generation 46

VII. Interactions and Technology Transfer 48

A. Industrial interactions 48
B. Interactions with DoD labs and other institutions 48

VIII. References 49

IX. Publications 52

X. Presentations 53

XI. Personnel 54

I. Introduction

Over the last two decades, there has been great interest in the development of techniques to generate and detect freely propagating pulses of coherent sub-millimeter wave radiation using ultrashort optical pulses from mode-locked lasers [1, 2]. These techniques use ultrafast optical excitation to produce either radiative current transients in photoconducting antennas or nonlinear polarization via optical difference frequency mixing in a variety of nonlinear media. Such frequency down-conversion schemes make it possible to access the wide range of frequencies within the baseband of an ultrashort optical pulse, which can easily extend out to several hundred cm^{-1} (1 THz = 33.33 cm^{-1} = 4.1 meV). Coupled with phase-coherent detection using either photoconductive or electro-optic sampling, these schemes of terahertz (THz) generation have provided powerful tools for time-domain far-infrared (FIR) spectroscopy [3] and THz imaging [4].

In studies supported by this research grant, we have investigated both the fundamental aspects and spectroscopic applications of optoelectronic techniques of generation and detection of sub-picosecond electromagnetic pulses. The original research objectives pursued under this grant included the development of significant new capabilities and an improved fundamental understanding of the physical mechanisms involved in the optoelectronic generation and detection of THz radiation. The characteristics of such optically excited THz emitters with respect to the scaling of their peak THz intensities using higher optical fluences and enhancements in their THz frequency response were also to be explored. One of the main issues addressed by these studies was the development of new bright coherent sources and sensitive detectors to enable linear and nonlinear spectroscopy in the far-infrared region of the electromagnetic spectrum.

During the period of time covered by this report, our accomplishments include the development of ultrafast laser-based techniques and new devices for generating and coherently detecting both free space and guided-wave THz radiation. The combination of an optoelectronically driven THz emitter and a synchronously gated optoelectronic detector, together with appropriate FIR optics, has been utilized to measure the linear optical properties of a variety of dielectric and semiconductor materials with exceptional sensitivity over a spectral range exceeding 100 cm^{-1} [1, 3]. Because of the gated nature of the phase-coherent detection process, the strong thermal background, which plagues traditional measurements in the far-infrared, is observationally absent [3]. As discussed below, significant progress has been made towards enhancing the performance and expanding the capabilities of such a system for time-domain far-infrared spectroscopy.

II. Key Accomplishments

The major accomplishments of our research efforts for the period of November 1, 1991 through April 30, 1996 are summarized below:-

- Development of a new large-aperture Si p-i-n diode for generating intense sub-picosecond electromagnetic radiation. The frequency response of such a THz emitter is not determined by the thickness of the intrinsic layer but by the transient dynamics of the photogenerated carriers within it. Thus, the device structure can be optimized for high quantum efficiency at the pump wavelength without sacrificing the THz frequency bandwidth.
- Study of transient electron dynamics in GaAs using optically induced THz radiation from large-aperture GaAs p-i-n diodes. The changes in the amplitude, duration and shape of the radiated THz fields as a function of the wavelength of the optical excitation and the reverse bias reflect the velocity overshoot property of the transient carrier dynamics in GaAs.
- Observation of Gunn oscillations by triggering an appropriately biased vertical transferred electron device (Gunn diode) with femtosecond optical pulses.
- Investigation of the dynamics of photoinjected carriers on sub-picosecond time scales by careful analysis of the radiated THz fields induced by sub-band gap optical excitation of bare semiconductor surfaces. For such non-resonant excitation, the major contribution to the generation of THz pulses is from the reactive photocurrent caused by the polarization of virtual carriers by the depletion field (field-induced optical rectification).
- A systematic study of the physical mechanism involved in the generation of THz radiation by femtosecond optical excitation of bulk GaAs. The experimental results reveal that both displacement and transport currents contribute to THz radiation and their relative contributions are highly sensitive to the dc electric field.
- Construction of a Ti:sapphire regenerative amplifier (pumped by a Q-switched frequency-doubled Nd:YLF laser) capable of producing 1 mJ, 150 fs pulses at 1 kHz. This system is being used for high intensity broadband and narrowband THz generation.
- Demonstration of a novel technique of generating tunable narrowband intense THz radiation in free space from large-aperture photoconducting antennas. This scheme relies on mixing two linearly chirped broadband optical pulses with a variable delay to produce a tunable quasi-sinusoidal intensity modulation.
- Generation and coherent detection of free space narrowband THz radiation using photoconducting dipole antennas tunable from 0.06 to 0.8 THz. The spectral selectivity of the narrowband emitter and the narrowband detector can be tuned independently.
- A detailed analysis of the chirped pulse beating process taking into account limitations imposed by the cubic phase in the chirped pulses. The numerical analysis agrees very well with cross-correlation measurements performed by optical second harmonic generation.

- Investigation of the saturation characteristics of the peak THz field emitted by planar photoconducting antennas with increasing optical fluence. We have shown that the chirped pulse mixing scheme can produce narrowband THz radiation with the highest possible spectral brightness from such structures.
- Generation of narrowband THz radiation from type II phase-matched difference frequency mixing in $LiNbO_3$ using femtosecond optical excitation. An FWHM bandwidth of ~10 GHz tunable over ~400 GHz was obtained.
- Generation of broadband THz radiation from a poled polymer. The coherence length for difference frequency mixing in this medium is a few mm for frequencies >15 THz, i.e., > 100 times larger than that of $LiNbO_3$ while the FIR absorption is ~10 times lower. This implies that these materials are ideal candidates for intense FIR emitters.
- The first demonstration of coherent detection of freely propagating THz radiation by electro-optic sampling in a poled polymer. This technique has the potential to significantly increase the detection bandwidth to >15 THz.
- Demonstration of an ultra-high bandwidth system for coherent THz spectroscopy based upon the use of non-resonant second-order nonlinearities, i.e., optical rectification and electro-optic sampling in <110> ZnTe crystals.
- Development and implementation of a non-perturbative probe of transient electric fields in high- speed silicon circuits and devices based on optical second harmonic generation. We have recently demonstrated the first measurement an ultrafast electrical pulse propagating on a coplanar transmission line with subpicosecond time resolution by SHG.

III. Optoelectronic Generation of THz Radiation from Semiconductor Devices

Substantial progress has been made in the area of generating broadband THz radiation from a variety of semiconductor devices. Such optically induced THz radiation is a powerful tool for obtaining valuable information on the sub-picosecond dynamics (such as transient mobility) of photogenerated carriers under applied fields in semiconductors, and hot carrier effects associated with them (such as transient velocity overshoot). THz generation provides a new optoelectronic technique to characterize the surface and interface electronic properties of semiconductors through the measurement of the amplitude and direction of the surface static field, doping type and dopant concentration, and even crystal symmetry. Our work in this area over the past few years is summarized in the following sections.

A. THz radiation from large-aperture Si p-i-n diodes:

One of the difficulties we encountered in our previous work on generating intense THz radiation from a large-aperture planar photoconducting antenna is the limited attainable bias field.

The highest bias field is determined not only by the breakdown voltage of the semiconductor material, but also the electrode contacts and the environment under which the experiment is conducted. Normally, the large-aperture photoconducting antennas we have used before can withstand only a moderate field (~ 2 kV/cm) which is much lower than the breakdown field of the material. To achieve higher bias fields and consequently, more intense electromagnetic radiation, we have initiated new research on the use of large aperture p-i-n diodes for generating directional and intense electromagnetic pulses with terahertz bandwidths. By applying a reverse bias, we can achieve a much larger bias field in the intrinsic region, which is close to the dielectric breakdown field of the semiconductor.

The p-i-n diode is one of the most common photodetectors because the depletion region thickness (the intrinsic layer) can be tailored to optimize the quantum efficiency and frequency response. As a photodetector, high quantum efficiency requires that the intrinsic layer thickness of p-i-n diode is larger than the photon absorption length. On the other hand, the high speed response requires a thin intrinsic layer for small transit times of photogenerated carriers through the this layer. For a conventional silicon p-i-n photodiode with 3 μm thick intrinsic layer, the 3-dB response frequency is ~10 GHz for 80% quantum efficiency at 615 nm. Here, we demonstrate that large aperture silicon p-i-n diodes can be used as emitters for THz beams. This occurs when we couple the signal out by radiating into free space, rather than coupling to the electrodes, as is done in a conventional photodiode. The generation of optically-induced THz radiation from semiconductor p-i-n structures is similar to that which we have previously reported from semiconductor depletion layers [5]. It is found that the amplitude and spectral bandwidth of the radiated pulses strongly depends on the reverse bias of the p-i-n diode. Unlike the frequency response of a conventional p-i-n photodetector, the frequency bandwidth of the radiated pulses from the large aperture Si p-i-n diode is not determined by the thickness of the intrinsic layer but by the transient process for the photogenerated carriers to reach steady state inside the intrinsic layer. Hence, the radiation frequency spectrum can extend to a few THz and the thickness of the intrinsic layer can be optimized for high quantum efficiency.

The Si p-i-n diodes used as terahertz radiation emitters were grown in a high vacuum Rapid Thermal Chemical Vapor Deposition (RTCVD) system. The carrier concentration in the intrinsic layer was less than $1x10^{12}$ cm^{-3} and was below the detection limit of the spreading resistance measurement. The ohmic contacts were fabricated so that an external bias could be applied as shown in fig. 1. The electric potential on the top layer (p^+ layer) is uniform due to its small sheet resistance (1000 Ω). However, this sheet resistance of top layer is large enough so that the absorption of the THz radiation in this layer is less than 5%. Measurements of the p-i-n diode C-V characteristics demonstrated that the capacitance was not dependent on the reverse bias, indicating complete and uniform depletion of the field inside the intrinsic layer. The p-i-n junction broke

down at about 43 V reverse bias (140 kV/cm electric field in the intrinsic layer). Since the absorption length of Si at 615 nm was about 2 μm and the depletion length in the heavily doped semiconductor was extremely small, almost all the photogenerated carriers were driven by the depletion field inside the intrinsic region to form a transient current. Hence, we can expect high quantum efficiency at this wavelength.

Fig. 1 schematically illustrates the set up of the experiment. The Si p-i-n diode is illuminated by femtosecond optical pulses from a balanced colliding-pulse modelocked (CPM) dye laser which produces 70 fs optical pulses at 615 nm with a 100 MHz repetition rate and 25 mW average power. The optical beam is split into two beams by a beam splitter. The unfocused pump beam illuminated the Si p-i-n diode at an incident angle of 60 degrees. The probe beam passed through a variable time-delay stage and was focused on a synchronously gated dipole detector to measure the temporal waveform of the radiated signals. The detector is placed 1.5 cm away from the Si diode along the direction of reflected optical beam.

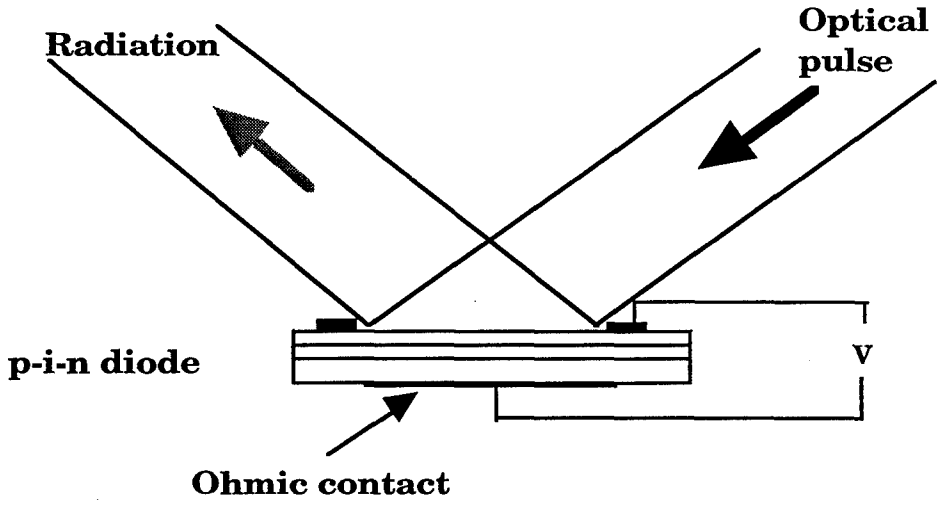

Figure 1

The radiated electric fields detected from the Si p-i-n diode under different bias fields are shown in fig. 2 (a). Some very interesting features can be seen from this figure. First, as the reverse bias increases, the peak value of the radiation field increases dramatically. The peak radiation field with 40 V reverse bias is more than 25 times larger than that without external bias and more than 50 times larger than that from the surface depletion field of a bare Si wafer. Secondly, as the reverse bias increases, the pulse width of the radiation field decreases and the time delay corresponding to the peak of the radiation field also decreases. When the p-i-n diode is in open circuit, the pulse width (FWHM) is 1.2 ps; when the diode is reverse biased at 40 V, the radiation pulse width decreases to 0.76 ps.

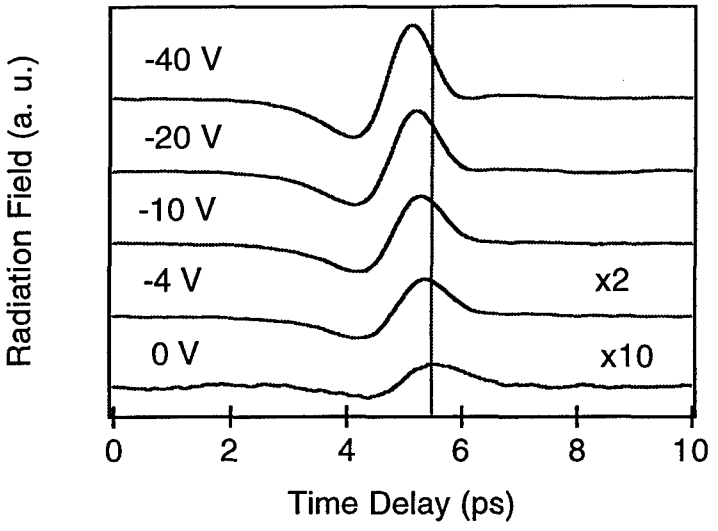

Figure 2a

Fig. 2 (b) shows the normalized spectrum of the radiation field under the corresponding reverse biases. The radiation spectrum clearly extends to higher frequencies as the reverse bias increases, which corresponds to a decrease in the radiation pulse width.

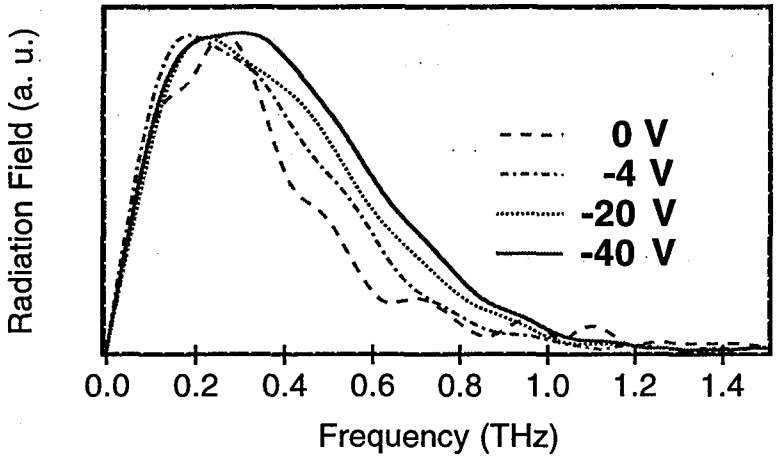

Figure 2b

In fig. 3, we show the detailed bias dependence of the peak radiation field. The radiation field increases linearly with the reverse bias at "low" fields (<15 kV/cm in the intrinsic layer), becomes sublinear as the field increases, and saturates at the extremely high fields (~ 130 kV/cm). This saturation feature is almost the same as that of the steady state drift velocity of electrons in silicon [6]. The peak amplitudes of the THz pulses have a constant value in the forward bias region, because a large forward bias cannot be applied to the intrinsic region due to the large forward current. However, if we extrapolate the E_p-V curve to the forward bias region, we find E_p=0 when V_0=+0.8 V which is approximately the same as the built-in voltage (0.85 V).

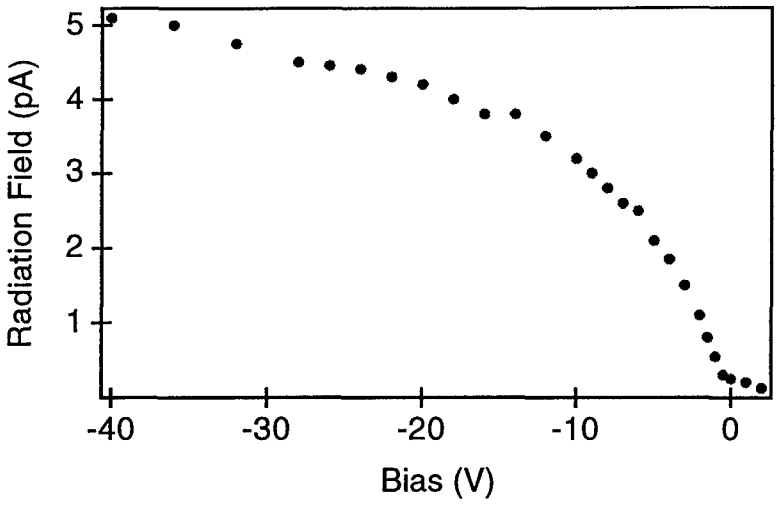

Figure 3

For comparison, we used a Si p-i-n diode with a 1 μm thick intrinsic layer as an emitter under the same experimental conditions. We found that the radiation signals were smaller than those from the 3 μm diode with the same depletion field. The smaller radiation signal can be explained by the low quantum efficiency because the thickness of intrinsic layer is smaller than the absorption length of optical pulse. However, the shape of the radiation signal and the field dependence of radiation amplitude for the 1 μm p-i-n diode are almost the same as the 3 μm diode under the same depletion field. Consequently, the frequency spectrum of the radiation field does not change with the thickness of the intrinsic layer.

To explain the experimental results above, it is necessary to understand the mechanism of the radiation generation by the optically induced carriers. The radiation field near the large aperture Si p-i-n emitter surface can be expressed as [7]:

$$E_r = \frac{\left(\int_0^d J dx\right)\sin\theta}{nc_0\varepsilon_0\left(n\cos\theta + \sqrt{1-n^2\sin^2\theta}\right)} \qquad (1)$$

where J is the transient current density induced by the optical excitation and the depletion field, d is the thickness of the intrinsic layer, n is the index of refraction at the radiation frequency and θ is the optical incident angle. The transient current density J is given by:

$$J(x,t) = \int_{-\infty}^{\infty} \frac{qI_{op}}{\hbar\omega_0} \exp\left(-\alpha x - \frac{t'^2}{\tau^2}\right) v_d(t-t', E)dt' \qquad (2)$$

where q is the electric charge of carriers, I_{op} is the peak intensity of the optical pulse, $\hbar\omega_o$ is the optical photon energy, α is the optical absorption coefficient, τ is the time duration of optical pulse (assumed to be Gaussian), v_d is the transient drift velocity of photogenerated carriers and E is the depletion field which is constant for the p-i-n diode. The transient behavior of photogenerated hot

carriers under high electric fields is complicated and typically requires Monte-Carlo simulations to obtain quantitative results [8]. If the hot carriers generated by the optical pulse have large excess initial energy (maximum of 0.88 eV for electrons in our experiment), they will have very large phonon scattering rates due to the energy dependence of momentum relaxation time. Thus the strong dissipation of energy of the carriers due to phonon scattering slows down the rise time of drift velocity v_d to about a picosecond [6, 8]. On the other hand, the optical pulse duration τ is so small (~70 fs) that the transient drift velocity v_d is virtually zero for $t' < \tau$. So the transient current can be written as $J = Nqv_d(t, E)$, where N is the number of carriers generated per unit area inside the intrinsic region per optical pulse. Then, the radiation field near the emitter surface is:

$$E_r = \frac{Nqv_d(t,E)\sin\theta}{nc_0\varepsilon_0\left(n\cos\theta + \sqrt{1-n^2\sin^2\theta}\right)} \qquad (3)$$

This formula gives a simple relation for the radiation field as a function of carrier density, incident angle of the optical pulse, and the transient velocity of the carriers. From eqn. (3), the radiation field near the emitter surface is directly related to the transient velocity of the photogenerated electrons, so the amplitude of the radiation field is proportional to the steady state velocity of the electrons. This is why the radiation amplitude has the same saturation feature as the steady state drift velocity of electrons in Si, which is shown in fig. 3, and the frequency spectrum of the radiation field does not change with the thickness of the intrinsic layer of p-i-n diode. It should be mentioned that the radiation signal is detected 1.5 cm away from the Si p-i-n diode. Diffraction causes the radiation waveform to become a pulse instead of a step function having a duration comparable to the rise time of the transient velocity of the carriers. However, the saturation properties are unchanged. Also, the shortening of the radiation pulse and the decrease in the time delay for the radiation to reach its peak value imply that the rise time of the transient velocity of the carriers decreases when the reverse bias on the diode increases. We also can estimate the radiation field from equation (2). By using $N \sim 3\times10^{10}$ cm^{-2} per pulse, $v_d \sim 10^7$ cm/s, n(Si)=3.42, $\theta=\pi/3$ and 0.1 cm^2 optical beam size, the estimated value of the radiation field near the emitter is ~2 V/cm. If we assume the rise time of the transient velocity is 1 ps, the radiation field after 1.5 cm propagation is a pulse with 0.7 V/cm amplitude and about 1 ps duration.

It is interesting to make some comparisons between externally biased semiconductor devices (including large aperture antennas [9])and semiconductor surfaces with internal depletion layer fields [5] for THz generation. First, compared to the semiconductor surfaces, the large aperture p-i-n diode is a more efficient radiation source because almost all of the photogenerated carriers can be confined inside the depletion field region by controlling the thickness of intrinsic layer. Secondly, the depletion region of the p-i-n diode provides a controllable uniform electric field while the other two techniques cannot. Thus, we can study the time dependence of the drift

velocity under different field strengths by applying different reverse biases. Finally, compared to the large-aperture planar photoconducting antenna which can only sustain bias fields of few kV/cm and needs a high voltage power supply, the large aperture p-i-n diode is able to produce higher bias fields (~140 kV/cm) with much lower bias voltages (~40 V). As the maximum possible radiation field is limited by the bias field at high optical fluences [10], the large aperture p-i-n diode is potentially capable of generating higher radiation fields at higher optical fluence.

In conclusion, we have generated subpicosecond electromagnetic pulses from large aperture Si p-i-n diodes by femtosecond optical excitation. The changes in amplitude and duration of these pulses under different reverse biases reflect the dependence of transient behavior of photogenerated carriers on the electric field.

B. Study of transient carrier dynamics in semiconductors using optically induced THz radiation:-

The emission of THz radiation from optically excited semiconductors takes place on a subpicosecond time scale, and the mechanism behind it is very complicated. While models based on either classical drift currents or field-induced nonlinear optical processes have been proposed, a complete theoretical understanding is still lacking. Nevertheless, the temporal waveform of the THz radiation clearly reflects the transient physical processes in the semiconductor. Therefore, by carefully analyzing the waveforms of the radiation generated under different experimental conditions, one can learn more about the carrier dynamics on such short time scales.

1. THz radiation induced by sub-band gap femtosecond optical excitation of semiconductor surfaces:- It has recently been independently proposed by Yamanishi [11] and Chemla *et al.* [12] that in a dc-biased multiple quantum well structure (MQW), a THz electrical transient can be produced by screening of the bias field by virtual electrons and holes induced by a femtosecond laser pulse tuned below the absorption edge. This does not require the generation of the real carriers, i.e. there is no energy deposited in the semiconductor. The term "virtual electron-hole pairs" refers to the valence charge fluctuations driven coherently by the intense laser field. Since there are no real collisions, this process is coherent, and consequently, very fast. It occurs on a time scale ~ $(E_g - \hbar\omega_{op})^{-1}$, where E_g is the band gap and $\hbar\omega_{op}$, the optical photon energy. Later, Yablonovitch *et al.* [13] extended this idea to bulk semiconductors and give it the name "virtual photoconductivity".

Our experiments on the THz radiation bulk GaAs sample excited with the photon energy tuned from above to far below the bandedge has given us more physical insight into this nonlinear process [14]. The THz radiation is induced from the depletion field region at the surface of the sample. Since the real current disappears with the decrease in the real absorption, by examining the THz radiation induced by different photon energies, we can make some assessment of the relative contributions from the two models to the generation of the THz signal.

Two tunable femtosecond lasers have been used in these experiments. One is a tunable dual-jet hybrid mode-locked Styryl 9 dye laser synchronously pumped at 76 MHz by a frequency-doubled Nd:YLF laser. The other is a self-modelocked Ti: sapphire laser cw-pumped by an Argon ion laser. In both cases, the laser produces 100 fs pulses with the wavelength tunable from ~800 nm to ~900 nm. The spectrum of the pulse has a full width at half maximum (FWHM) of ~12 meV. Fig. 4 shows the schematic of the experimental set up. The bulk GaAs sample is placed in a cryogenic dewar. A photoconducting dipole detector is located at the specular angle of reflection, about 2 cm away from the sample which ensures detection in the far-field.

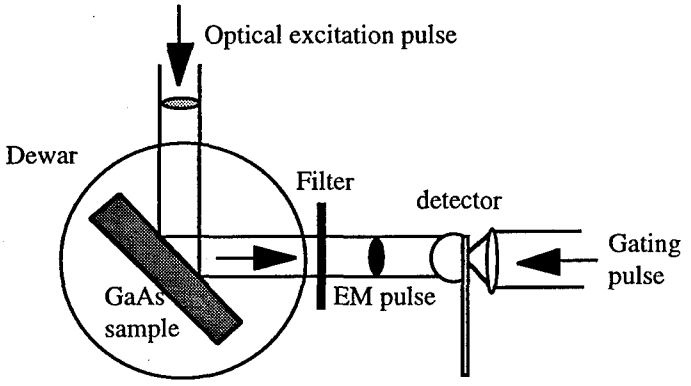

Figure 4

The measurement is done in the same way as described in section III.A. One portion of the unfocused laser beam is used to illuminate the bulk GaAs sample to induce THz radiation. A probe beam, which passes through a variable delay, and is focused down to gate the 100 μm dipole detector. The temporal waveform of the radiation is mapped out as a function of the relative time delay between the two beams.

One of the important issues in the experiment is the width of the photon energy spectrum relative to the band edge. Due to the Urbach tail, at room temperature, the band edge is very broad, and becomes sharper at lower temperature [15]. Therefore it is necessary to perform the measurement at low temperature. Normally, we cool the sample to about 100 K. In order to check temperature effects, we also performed the same measurement at different temperatures. The experiments are carried out at 110 K on an undoped semi-insulating GaAs wafer with a thickness of 400 μm. The optical beam strikes the sample at an angle of about 40 degrees with respect to the normal. The average pump fluence is low (~3 nJ/cm^2), so that density dependent effects and space charge effects are small.

Fig. 5 shows several of the radiated waveforms. $\delta\varepsilon$ denotes the energy difference between the photon energy at the center of the laser spectrum and the bandgap. These waveforms show some very interesting features. When the photon energy is well above the band gap, the signal has a very large amplitude with a negative main peak, and the amplitude does not change much with the

photon energy. As the photon energy is tuned towards the band edge, the amplitude starts to decrease. It drops very quickly down to almost zero, as the photon energy passes through the band edge. At this point, a very dramatic change occurs. The radiated waveform reverses its sign with its main peak changing from negative to positive. This sign reversal is very dramatic depending on the sharpness of the bandedge. At 110 K, this happens when $\delta\varepsilon$ is tuned by only about 3 meV. However, at 200 K, this happens rather slowly. In both cases, the sign reversal occurs when the absorption is reduced by more than an order of magnitude.

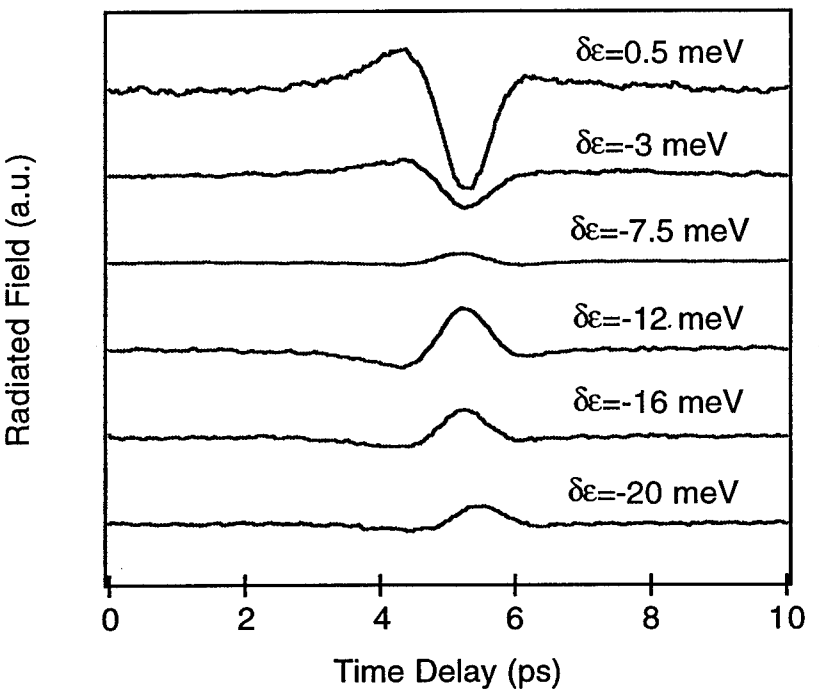

Figure 5

After the sign reversal, as $\delta\varepsilon$ is further decreased, the waveform is unchanged. However, the amplitude slightly increases and then decreases again at a much slower rate compared to the decrease near the band edge. Fig. 6 shows the amplitude of the radiated signal versus the detuning energy. The signal is still apparent even when the photon energy is 40-50 meV below the bandgap. To gain more insight from the experimental results, first, consider the radiation from a real photocurrent. In the far field region, the temporal waveform should follow the negative first time derivative of the transient photocurrent. It can be roughly estimated with an assumption about the time dependence of the transient current. In our case, the depletion width is roughly several μm, and the static depletion field is estimated to be about a few kV/cm. Wysin *et al.* made a detailed Monte-Carlo calculation of the transient photocurrent in GaAs [16]. Their results suggest that for GaAs (under a bias field of ~ 5 kV/cm) illuminated by a femtosecond laser pulse with a center photon energy of 1.5 eV, the photocurrent will rise very quickly, in about 200-300 fs, reach an overshoot value, then gradually decrease, and relax down to the normal steady state value on a

picosecond time scale. The first time derivative of the transient current will have a sharp positive peak followed by a small slow negative lobe. Therefore, the main peak of the radiated signal will be negative. Using the numerical values from their paper, we estimate that the amplitude of the detected radiation would be on the order of a few V/cm for excitation above the band gap. This is close to what we detected in the experiment. For excitation near or just below the band edge, the signal should drop very quickly, since the optical absorption decreases exponentially [15]. This is consistent with fast decay of the signal as $\delta\varepsilon$ is tuned through the band edge as shown in fig. 6.

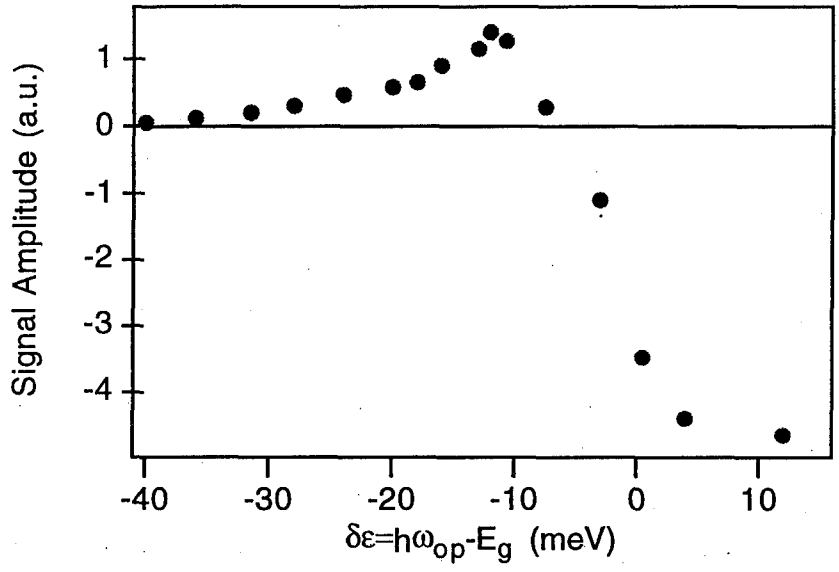

Figure 6

When the photon energy is tuned well below the band gap, the real photocurrent diminishes. However, as described by Yamanishi, Chemla *et al.*, and Yablonovitch *et al.* [11-13], there is a reactive photocurrent caused by the polarization of the virtual photocarriers, which can be described by a third order nonlinear polarization:

$$P^{NL} = \chi^{(3)}(0;0,\omega_{op},-\omega_{op})E_{op}(\omega_{op})E^{*}_{op}(\omega_{op})E_{dc} \qquad (4)$$

where $\chi^{(3)}(0; 0, -\omega_{op}, \omega_{op})$ is the nonlinear susceptibility due to the inverse Franz-Keldysh effect. For a bulk GaAs sample assuming an abrupt band edge, Yablonovitch has obtained the following simplified expression:

$$\chi^{(3)}(0;0,-\omega_{op},\omega_{op}) = \frac{1}{24\pi^2}\frac{e^2\alpha cn}{E_g m_{eff}}\left(\frac{h}{\Delta}\right)^3 \approx \frac{1.46\times10^{-3}}{\Delta^3}\text{esu} \qquad (5)$$

where Δ is the detuning energy: $\Delta=E_g-h\omega_{op}$ in meV [13].

This nonlinear polarization has the spatial and temporal dependence of the optical excitation pulse. Clearly it is enhanced by the near resonance excitation. The far field waveform induced by $\mathbf{P}^{NL}$ should follow the negative second time derivative of $\mathbf{P}^{NL}$. The radiated waveform would have a large main peak with two small lobes of the opposite polarity. The polarity of the main peak is the

same of that of $\chi^{(3)}$ which is positive. Therefore, the main peak of the radiated waveform generated by the transient photocurrent should have an opposite polarity to that generated by the nonlinear polarization model. Furthermore, the current contribution is linear with the optical absorption, and decreases exponentially as the photon energy is tuned through the bandedge. The sign reversal and the different rate of change in signal amplitude as a function of the photon energy in our experiments clearly suggest a competition between transient photocurrents and nonlinear polarization as the dominant mechanism generating THz radiation.

In all cases, some real absorption probably existed, due to the tail states and impurities within the depletion region. However, at 110 K (20-40 meV below the band edge of GaAs), the optical absorption should have been negligibly small. To check how far the optical pulse propagates in the crystal, we made a very thin sample with a thickness of only 100 μm. We expect that as the optical pulse passes through the sample, it should generate THz radiation both in the depletion region at the front surface and the depletion region at the back surface. The pump beam was aligned at Brewster's angle, so that the THz signal generated at the front surface was not reflected by the back surface.

Fig. 7 shows some of the waveforms we obtained from the thin sample. For $\delta\varepsilon$=-7 meV and -15 meV, the waveform is clean and no reflection by the back surface is observed. However, when $\delta\varepsilon$ is 50 meV below the bandedge, we see a second peak emerging 2 ps later with an opposite polarity to the first peak. The time delay between the two peaks exactly matches the time that the THz signal generated at the back surface needs to travel back to front surface. This strongly suggests that at 50 meV below the band edge, the absorption is negligible, as the effects due to the real carrier drift cannot explain the amplitude of the observed THz signal. The signal is then mainly due to optical rectification.

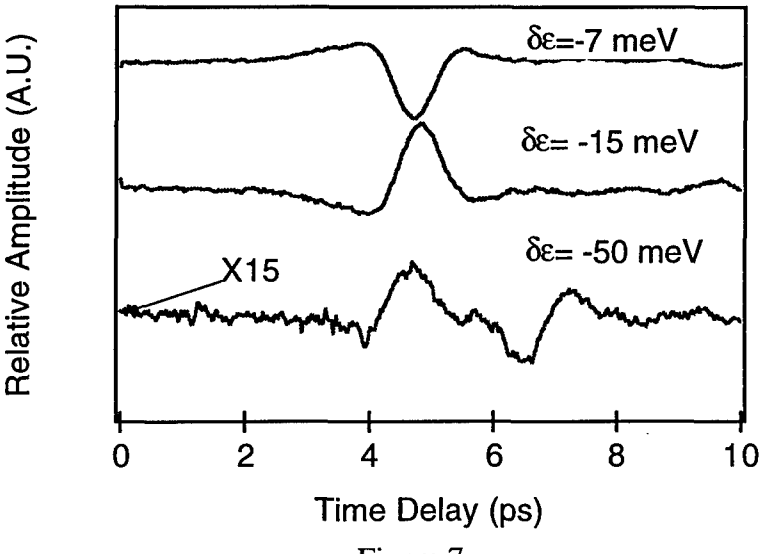

Figure 7

To further prove the point, we also measured the signal dependence on crystal orientation. We changed the optical polarization and then monitored the amplitude change of the radiation signal. For above band gap excitation, the THz radiation did not show any dependence except that due to Fresnel losses at the interface. This was double checked at room temperature with the crystal rotated azimuthally about its surface normal. No orientation dependence was found in all cases.

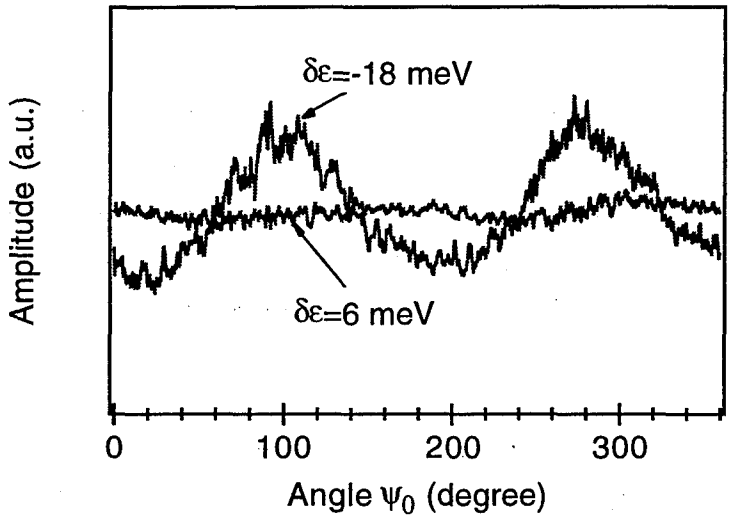

Figure 8

For sub-bandgap excitation, however, as we change the optical polarization, we observe a large modulation of the THz radiation amplitude. This follows from the fact that $S \propto \mathbf{d}\cdot\mathbf{P}^{NL}$, where S is the radiated field strength and **d** is the unit vector parallel to the dipole axis. This can be expressed as:

$$S = F(\psi_i,\theta_i,\theta_r)[(\chi_{xxyy}+\chi_{xyxy})+(3\chi_{xxxx}\sin^2\theta_r-\frac{(\chi_{xxyy}+\chi_{xyxy})}{2n} \quad (6)$$
$$(\cos(\theta_i+\theta_r)+3\cos(\theta_i-\theta_r)))\cos^2\psi_r$$

where the indices i, and r indicate the incident and refracted beam respectively, $\theta_{i(r)}$ is the incident (refracted) angle, ψ is the angle between the optical polarization in the surface plane and the crystal orientation (100), and F is the corresponding Fresnel coefficient. Experimental results for $\delta\varepsilon$=+6 meV and $\delta\varepsilon$=-18 meV are shown in fig. 8.

This experiment has demonstrated radiation generated by a sub-bandgap excitation. It also shows a transition in the dominant radiation contribution due to the two models proposed. However, there is one unknown factor, i.e. the strength of the depletion field. For undoped semi-insulating GaAs, it is very difficult to determine the exact magnitude of the depletion field. The sample we used in the above experiment is believed to have a very small depletion field. We

roughly estimate it to be ~ 1 kV/cm, by comparing the signal strength generated from the sample with that from a p-i-n diode.

2. Transient velocity overshoot effects observed in THz radiation from GaAs p-i-n diodes:- We have demonstrated that p-i-n diode provide useful methods for studying the transient behavior of carriers in photoconducting materials. In the following section, we report the study of transient electronic processes by optically inducing terahertz radiation from a large aperture GaAs p-i-n diode. The GaAs p-i-n diodes used as terahertz radiation emitters in this experiment were grown by MBE. After a 1 μm n^+ GaAs buffer layer was grown on a n^+ GaAs substrate, a 3000 Å intrinsic GaAs ($<10^{15}$ cm^{-3}) layer was grown on top of the buffer layer. This was followed by a 200 Å p^+ doped contact layer with 8000 Ω sheet resistance. The ohmic contacts were fabricated so that an external bias could be applied. Due to the low doping level of the intrinsic layer, we expect complete depletion of the intrinsic region and uniformity of the depletion field inside the 3000 Å intrinsic layer. The p-i-n broke down at 5.0 V reverse bias (210 kV/cm electric field in the intrinsic layer).

The set up of our first experiment for a large aperture GaAs p-i-n diode is identical to that for a Si p-i-n described above [7]. Two femtosecond laser sources are used to produce terahertz radiation and gating the THz detector. For the first set of measurements, the optical excitation source is a CPM dye laser operating at 620 nm. The unfocused pump beam illuminates the GaAs p-i-n diode at an angle of incidence of 60 degrees. The other beam passes through a variable time-delay stage and is focused on the detector to measure the temporal radiation signals. The detector is a radiation damaged silicon-on-sapphire dipole antenna.

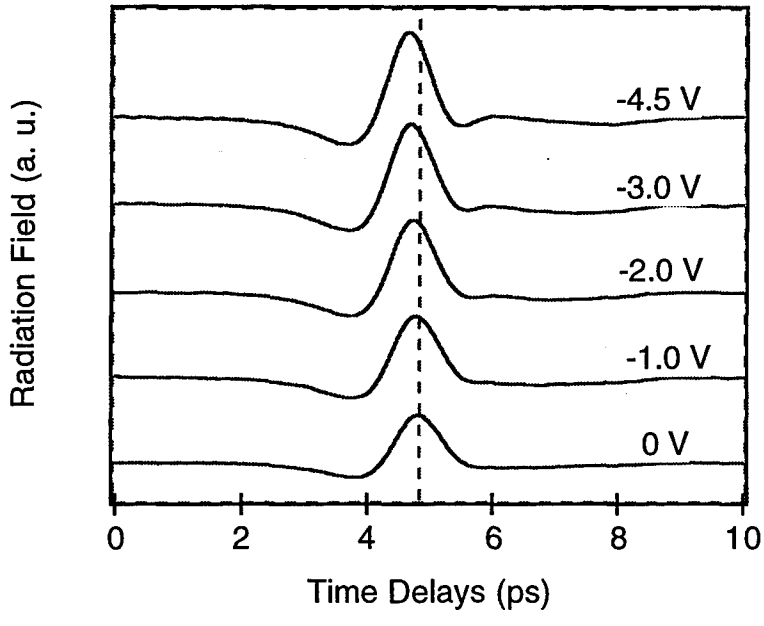

Figure 9

The time resolved radiated electric fields detected from the GaAs p-i-n diode at room temperature under different biases are shown in fig. 9. Some important features can be seen from this figure. First, as the reverse bias increases from 1 V to -4.5 V (which corresponds to an electric field of 13 kV/cm and 200 kV/cm, respectively), the peak value of the radiation field increases by about 75%. Secondly, as the reverse bias increases, the pulse width of the radiation field decreases from 0.62 ps to 0.57 ps, and the delay time for the radiation field to reach its peak point also decreases. The shift of peak of the radiation pulse is about 0.2 ps in this process. The spectrum of the radiation field in fig. 9 extends to higher frequencies as the reverse bias increases, which corresponds to a decrease in the radiation pulse width.

Fig. 10 shows the radiation signals from the Si p-i-n and GaAs p-i-n respectively under the illumination of the CPM laser (620 nm).The depletion field in the intrinsic layer of both p-i-n diodes is about 130 kV/cm. The radiation waveforms from both diodes are basically unipolar, but the radiation signal from GaAs is faster and its waveform has a small but significant dip after the main pulse as compared to that of Si.

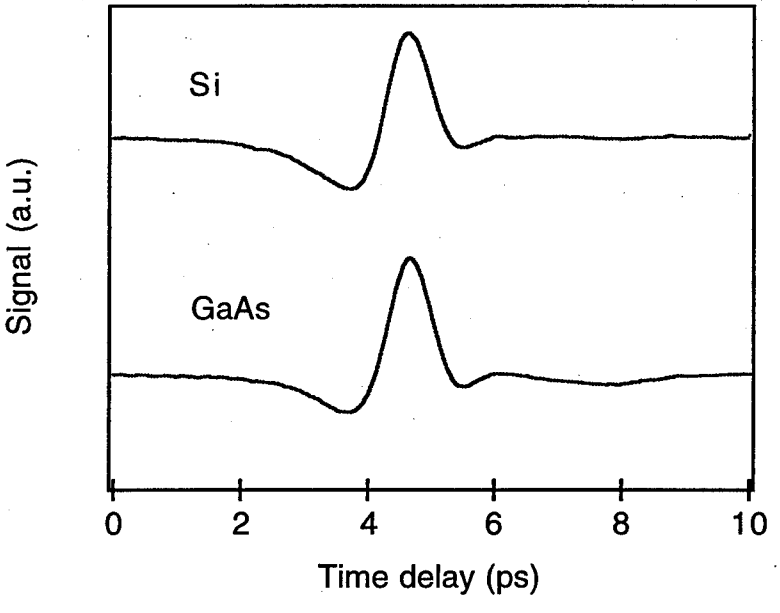

Figure 10

Velocity overshoot of electrons in GaAs is expected to be stronger when the photoexcitation is closer to the conduction band edge [16]. Thus, it is desirable to repeat the experiment at lower excitation photon energy. In the second experiment, the optical excitation source is a Ti:Al_2O_3 modelocked laser. The experimental set up is the same as the one using the CPM laser.

Fig. 11 shows the radiation signal from the Si p-i-n and GaAs p-i-n diodes under the illumination of Ti:Al_2O_3 modelocked laser (810 nm) with the same experimental set up, where the

average power of the laser beam illuminating the diodes is 300 mW. The depletion field in the intrinsic layer of both p-i-n diodes is about 130 kV/cm.

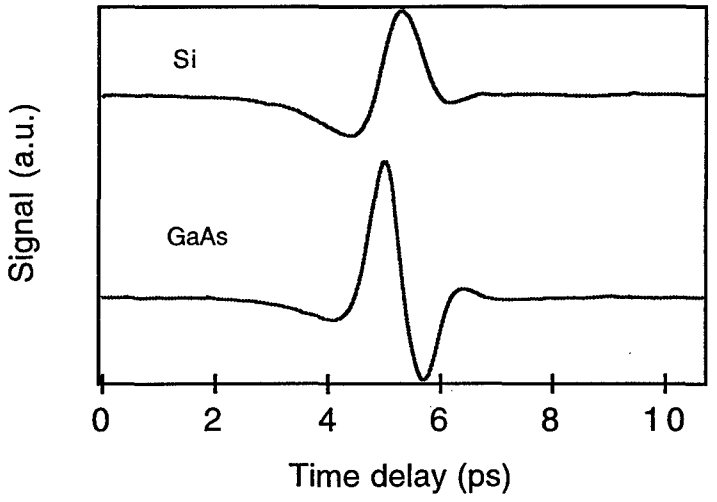

Figure 11

The amplitude of the radiation from GaAs is about 8 times larger than that from the Si diode. The pulse width of the radiation from the GaAs diode is 0.50 ps which is also the limit of the detector response. It is very interesting that the radiation signal is insensitive to the bias on the GaAs diode. Compared to the radiation signals generated by 620 nm illumination, the radiation signal from the GaAs diode now is noticeably faster and the pulse shape is significantly changed, while the waveform of the radiation from Si diode is almost unchanged.

From the transport current model, the radiation field near the emitter surface is directly related to the transient velocity of the photogenerated electrons [7]. Therefore, the hot electron transient dynamics in GaAs determines the characteristics of the radiation signal from the diode. The transient behavior of hot electrons photogenerated by short optical pulses in GaAs under electric fields has been studied both experimentally [17] and by Monte-Carlo simulations [16]. An important feature predicted by Monte-Carlo simulations is the well known velocity overshoot, i.e. under high electric field and low photon energy, the peak velocity of the electrons will exceed the steady state drift velocity before relaxation by phonon emission. But the experimental observation of velocity overshoot is difficult. The results of previous experiments using high optical fluences [17] on overshoot response on picosecond time scales has been interpreted in terms of charge-separation effects [18]. Also, a uniform electric field is difficult to achieve in experiments in which case geometrical effects may be important. However, under our experimental conditions, the photogenerated carrier density is less than $10^{15}/cm^3$, and the radiation pulse is linear with respect to the optical power, which indicates no band filling, carrier-carrier interaction, or space charge effects on the radiation process [19]. For THz radiation from the GaAs p-i-n diode, we believe that velocity overshoot of electrons explains the experimental results.

For GaAs, the most important features of the velocity overshoot are the dramatic increase of the peak transient velocity with the decrease of optical photon energy and the transient waveform of the drift velocity. We expect a change in the radiation waveform when we reduce the photon energy of the optical excitation pulse from 2.0 eV (CPM dye laser) to 1.54 eV (Ti:Sapphire laser). Under a 130 kV/cm bias field, the amplitude of the radiation field from the GaAs diode illuminated at 810 nm is 8 times larger than that at 620 nm if we use the amplitude of the radiation field from the Si p-i-n diode as a reference. By considering the optical absorption lengths at different optical wavelengths, the radiation field per electron from GaAs with 1.54 eV photoexcitation (810 nm) is about 5 times larger than that with 2.0 eV photoexcitation (620 nm). Thus the peak value of the average transient velocity of GaAs with 1.54 eV photoexcitation should be about 5 times larger that with 2.0 eV photoexcitation, which is in agreement with the numerical simulations. Although the simulations extend to only 50 kV/cm bias field, our comparison is still believed to be valid, because of the saturation behavior of velocity overshoot under high bias fields at both optical wavelengths.

For the case of radiation from the GaAs diode by 620 nm (2.0 eV) excitation, the significant feature is the dip after the main pulse. Since the radiation waveform from Si has no such feature and the corresponding transient velocity is a well known monotonically increasing function, we attribute this dip after the main pulse to a weak velocity overshoot. As the depletion field increases and the overshoot effect becomes stronger, this feature becomes more obvious as shown in fig. 9. Velocity overshoot in GaAs is usually a very fast process (less than 0.5 ps for 2.0 eV optical excitation), so that the corresponding radiation signal is faster than that from Si, which lacks the velocity overshoot feature. As the photoexcitation energy decreases, the dip after the main pulse due to velocity overshoot becomes larger, and finally, the radiation waveform becomes bipolar.

Velocity overshoot can also explain the bias dependence of the radiation pulse. Unlike the case of the Si p-i-n diode [7], the amplitude of radiation signal from the GaAs p-i-n diode does not have the same features as the steady state drift velocity of electrons in GaAs. It is well known that the steady state drift velocity of electrons in GaAs decreases with increasing electric field above 3.5 kV/cm at room temperature. At 2.0 eV optical excitation and room temperature, the onset of velocity overshoot starts at about 20 kV/cm [16], and the peak transient velocity increases slowly with the field which explains the increase of the radiation signal with the increase of the depletion field. When the photon energy is 1.56 eV which is slightly above the bandgap of GaAs, the overshoot velocity will saturate at about 5×10^7 cm/s when the electric field is above 20 kV/cm which is about the smallest field in the GaAs diode in our experiment. This is why the amplitude of the radiation signal is insensitive to the bias.

By using the Si signal as a reference, we can obtain a quantitative picture of the transient velocity of GaAs under photon excitation from the THz radiation. In the frequency domain, the detected radiation signal from large aperture p-i-n diode can be expressed as a convolution, $E(\omega)=R(\omega)v_d(\omega)$, where $R(\omega)$ is the response function including the effect of detector response and the propagation of the radiation and $v_d(\omega)$ is the ensemble average of transient velocity. $R(\omega)$ is the same for different radiation sources if the optical set up is identical. Now, it is easy to see that the transient velocity of GaAs can be expressed as:

$$v_{d,GaAs}(\omega) = \frac{E_{GaAs}(\omega)}{E_{Si}(\omega)} v_{d,Si}(\omega) \qquad (7)$$

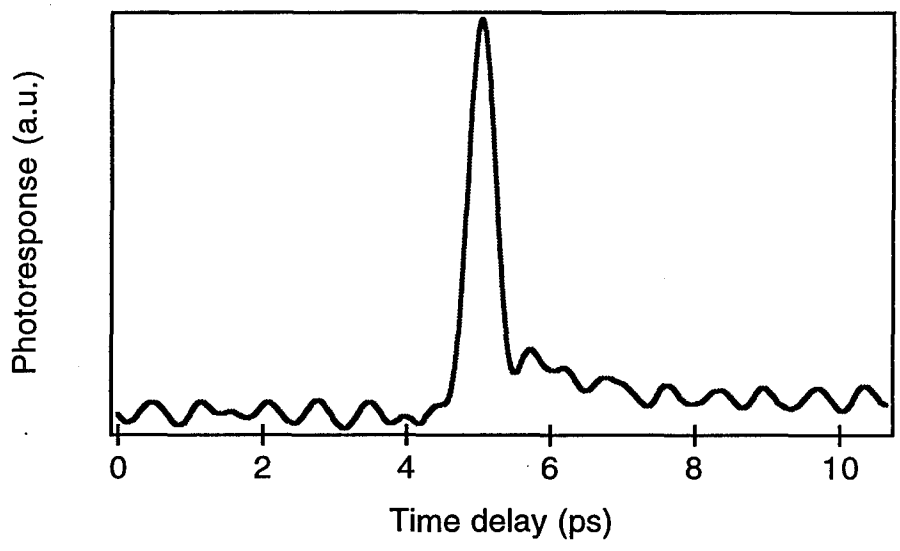

Figure 12

Therefore, once we have the radiation signal from the Si and GaAs diodes under identical optical alignment, we can derive the transient velocity of GaAs from the transient velocity of Si. From the Monte-Carlo simulations [8] and the radiation pulse width of Si, we assume the transient velocity of Si under an electric field of 130 kV/cm and optical excitation at 810 nm is a step function with a 0.5 ps rise time. In fig. 12, the calculated transient velocity of GaAs under an electric field of 130 kV/cm and optical excitation at 810 nm is shown. The velocity overshoot feature is very clear and the transient time for velocity overshoot is 0.45 ps.

In conclusion, we have generated THz subpicosecond electromagnetic pulses from large aperture GaAs p-i-n diodes by femtosecond optical excitation. The changes in amplitude, duration and the shape of these pulses under different optical wavelengths of excitation and different reverse biases on the p-i-n diode reflect the velocity overshoot property of the photocarrier dynamics.

C. Study of the physical mechanism of optically induced THz radiation:-

Recently, two conflicting explanations have been proposed for the origin THz radiation induced by femtosecond optical excitation of surface depletion layers of semiconductors. One

states that the photoexcited carriers are accelerated by the depletion field that exists near the surface producing a time-dependent transport current that radiates as a Hertzian dipole [5]. The other model proposes that the correlated photogenerated electron-hole pairs are polarized by the dc electric field and give rise to a time-dependent polarization in the depletion layer, whose time derivative is the displacement current that can also emit electromagnetic radiation [19]. Yet another source of the displacement current exists in non-centrosymmetric crystals such as GaAs where a direct second-order nonlinear optical difference-frequency mixing can also result in "optical rectification" of the excitation pulse even in the absence of the symmetry-breaking depletion field [20].

In an MQW structure, since the carrier transport is prohibited by quantum confinement, THz radiation induced should be caused only by the displacement current [21]. In bulk material, however, the physical picture becomes more complicated since both the transport and the displacement currents exist and contribute to THz radiation. Distinguishing the effects of the two mechanisms in a bulk sample has been hampered by the lack of systematic experiments. One of the difficulties in analyzing the THz radiation from bulk material is the uncertainty of the surface depletion field. The experimental results vary for samples with different surface fields [14, 22]. In previous experiments, for some GaAs samples, the THz waveform showed a sign reversal with the photon energy tuned around the bandedge, while for some other samples, no change in the THz waveform was observed [22].

To gain a better understanding of the physical mechanisms involved, a systematic study of the dependence of THz radiation on the dc electric field and the excitation photon energy is necessary. Here, we present the results of our recent experiments on a bulk GaAs sample. The MBE-grown sample we have used is shown as an inset in fig. 13. It consists of a 1.2 μm thick intrinsic GaAs layer sandwiched between two undoped 3500 Å thick $Al_{0.4}Ga_{0.6}As$ layers, on top of which there is a 200 Å GaAs capping layer followed by a 50 Å Cr film. The external bias field can be applied between the semi-transparent Cr contact on the sample surface and the n^+ GaAs (100) substrate. A similar design was used in ref. 6 for study of the field dependence of THz radiation in MQW structures.

The sample is placed in a cryostat, and is illuminated by an unfocused laser beam from a self-modelocked Ti: Sapphire laser with a pulse duration of 150 fs, a spectral FWHM of 7 nm, and a repetition rate of 76 MHz. The laser center wavelength is tunable around 800 nm, which enables the study of THz radiation at different photon energies. The photocarrier density is held at around $10^{12}/cm^3$ to avoid space charge effects in the GaAs layer. The induced THz radiation is measured by a photoconductive dipole antenna detector [23, 24], which is optically gated by a split-off portion of the laser beam which passes through a variable time delay. The detector is placed in the direction of specular reflection, 4 cm from the sample, thus ensuring detection of the far-field electromagnetic radiation. The ion-implanted Si-on-sapphire detector had a time resolution of 0.5

ps and a corresponding frequency response extending beyond 2 THz. To increase the sensitivity of the detection, a hemispherical sapphire lens was attached to the sapphire substrate of the dipole detector [24]. The radiation waveform was detected by recording the photocurrent from the dipole antenna while changing the relative time delay between the pump and the gating pulses. Since the detection scheme is coherent; both the amplitude and phase information of the radiation are recorded. The detected waveform is a convolution in the time domain of the radiated field and the detector response, therefore, changes in the shape and the amplitude of the temporal waveform should reflect the physical properties of the radiative source.

In the first set of experiments, we fixed the laser center wavelength at 785 nm which was approximately 80 meV above the bandedge of GaAs at a temperature of 120 K. We then varied the bias field, and measured the induced THz radiation. The waveforms showed no noticeable changes in shape. Fig. 13 shows the amplitude of the THz signal versus the dc bias field. The amplitude of the signal demonstrated a linear field dependence in the low field region. When the bias voltage was -0.65V, which was close to the flat band condition, the THz signal almost disappeared. This indicates the THz radiation observed here is mostly caused by field-induced effects, and the intrinsic bulk $\chi^{(2)}$ effects are small. In the high field region, this dependence becomes sublinear, and the signal amplitude saturates when the field reaches about 10 kV/cm. This type of saturation has been observed previously in a GaAs p-i-n sample [25] and a MQW sample [21] and was interpreted in terms of the transport and displacement current models, respectively.

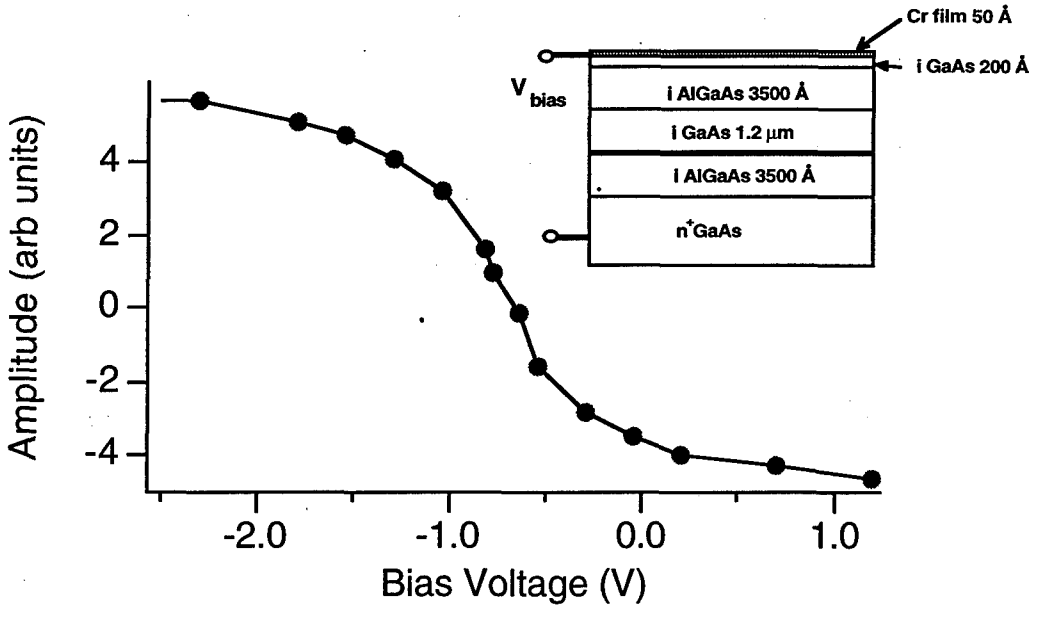

Figure 13

In the second set of experiments, we fixed the bias field at different values, and scanned the laser wavelength about the bandedge of GaAs. In fig. 14, the solid curves are the THz waveforms measured under a dc field of about 3 kV/cm and a sample temperature of 120 K, where $\delta\varepsilon$ is the

detuning energy, i.e. the energy difference between the photon energy and the band gap. The waveform changes drastically with the detuning energy. When the laser energy is tuned below the band edge, the radiated waveform has a negative main peak. The strength of the signal changes with the detuning energy, and reaches a maximum around bandedge. As $\delta\varepsilon$ is increased further, the negative main peak decreases, and a positive peak starts to develop. Interestingly, when $\delta\varepsilon$ is close to one LO phonon energy, which is 36 meV for GaAs, the THz waveform has a very small amplitude with some fine structure. Eventually, the waveform changes polarity as the positive peak develops and becomes dominant.

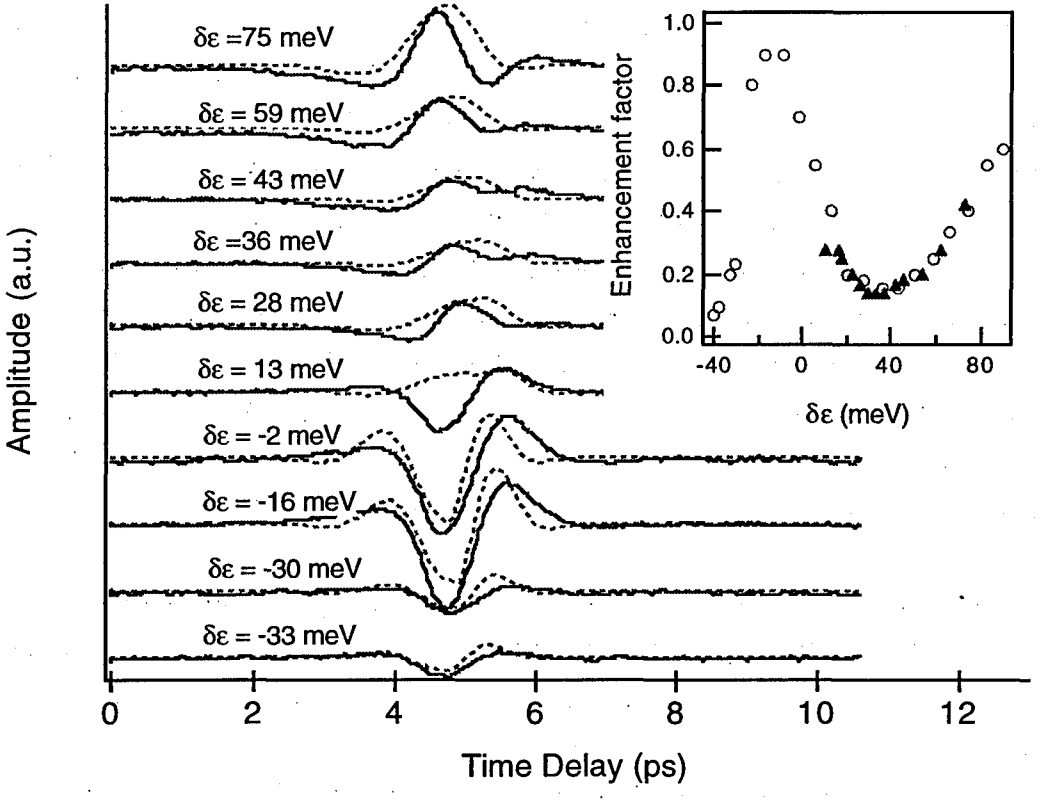

Figure 14

This polarity change of the radiation waveform with the detuning energy is very similar to the case we observed previously in an unbiased GaAs wafer [14]. According to the transport current model, the far field radiation should follow the first time derivative of the photocurrent. In our case the photocurrent is expected from a Monte-Carlo simulation to increase rapidly reaching an overshoot value in a few hundred femtoseconds, and then relax down to a steady state value in a few picoseconds [16]. The degree of overshoot depends on the photon energy and the dc electric field. The radiation waveform is expected to change slightly with the photon energy due to the different amounts of velocity overshoot. However, in general, the first time derivative of the photocurrent would have a positive main peak followed by a small negative lobe. The velocity

overshoot will only affect the small negative lobes in the radiation waveform. In experiments, this change is less obvious because of the relatively slow detector response. No polarity change with respect to the detuning energy is expected from this model.

The displacement current model requires the radiation waveform to follow the second time derivative of the nonlinear polarization [19]. According to ref. 19, the time dependence of the nonlinear polarization should have the time envelope of the optical pulse which is independent of the photon energy. The second time derivative of the polarization would give a symmetric temporal waveform with a negative main peak and two small positive lobes. Therefore, the two models predict two different time dependencies of the radiation field and the polarity of the radiated waveform has an opposite sign. Neither the transport current model, nor the displacement current model alone can explain such a waveform change. The sign reversal of the radiation signal suggests a competition between the displacement and the transport currents for inducing radiation.

The theory of the carrier transport during and at early times after the optical excitation should be able to describe the generation of polarized pairs as well as the translational motion of the carriers in the dc field. Neither the traditional semi-classical approach to carrier transport nor the steady-state quantum mechanical treatment proposed in ref. 19 are capable of this. As it has been demonstrated recently [26], one has to perform a full time-dependent quantum mechanical calculation to be able to describe both effects at the same time. According to ref. 26, the optical excitation creates carriers in localized wavepacket states rather than stationary eigenstates. These wavepackets move in the dc field and produce the transport current, but they are also polarized by the field which leads to the displacement contribution to the total current.

This theory is qualitatively consistent with our experimental findings because it predicts that the relative contributions of transport and displacement current effects depend on the detuning, the dc field and the pulse duration. At high positive detunings the transport part of the current is found to be dominant, while at negative detunings there is only the displacement current carried by the virtual carriers. The theory predicts a crossover from displacement-dominated to transport-dominated behavior as the excitation frequency increases, which we believe is the main reason for the observed sequence of waveform changes.

In fig. 14, the dotted curves are the theoretical fit to our experimental data. However, the direct comparison of the theory with the experimental data is complicated by a number of factors. The response function of the detector is not known, and for the purposes of this study we have assumed it to have the form:

$$R(t) = \cos\left(\frac{\pi t}{15}\right)\begin{cases}\exp\left[-(t/0.7)^2\right], t < 0\\ \exp\left[-(t/1.0)^2\right], t \geq 0\end{cases} \qquad (8)$$

where t is the time in units of ps. This response function is an empirical fit to the waveform at high positive detunings. Our choice of this function is based on the fact that the response function should be the detected waveform radiated from a step-function photocurrent, and the theoretical prediction that at high detuning the transport current, which can be approximated as a step function, is the dominant radiation source. A different choice of the response function will only affect the details of the theoretical fit. The main features such as the polarity reversal are basically independent of the response function. Since the theory only treats free electrons [26], we included scattering phenomenologically by introducing an exponential decay of the signal with the time constant of 150 fs.

The theory also does not include excitonic effects which can be expected to enhance the density of states near the band gap. To account for this effect, we have introduced a phenomenological detuning-dependent enhancement factor (see inset in fig. 14) to match the amplitude of the experimental and theoretical waveforms. This enhancement factor appears to have a dip at approximately one LO-phonon energy above the band gap which roughly accounts for the effect of scattering which is also not included into the model explicitly [26]. A comparison of the solid and the dotted curves in fig. 14 shows that the theory reproduces the observed sequence of waveforms reasonably well which confirms our initial suggestion that the change in the waveforms is due to the competition between the transport and the displacement current effects. There is, however, a considerable discrepancy between the theory and experiment around one LO-phonon energy above the gap which indicates that the onset of scattering requires a more accurate treatment.

One of the important features of the theory is its claim that the displacement contribution decreases with the dc electric field. The dc field not only pulls the virtual carriers apart, but also restructures the electronic wavefunctions. It turns out that the net result is the decrease of the displacement current with the dc field [26]. On the contrary, the transport contribution increases linearly with the field. Considering the scattering processes involved, the transport contribution may increase sublinearly and eventually saturate in the high dc field region [16]. Because of this unexpected non-perturbative result, at high fields the contribution from the transport current dominates. The time dependence of the transport photocurrent in this case, according to the Monte-Carlo simulation by Wysin et. al. is not expected to have dramatic changes with the photon energy [16]. Therefore, no significant waveform change in THz radiation with the photon energy should be observed. We have also carried out the same measurement at different dc bias fields. As we increase the dc field, the change in the THz waveform about the band edge gradually diminishes. When the dc field is approximately 10 kV/cm, no noticeable change in shape of the radiated waveform is observed. Fig. 15 shows the results for a bias field of 10 kV/cm and sample

temperature of 120 K. The amplitude of the signal again shows an enhancement near the bandedge due to excitonic effects. This is again in agreement with theory.

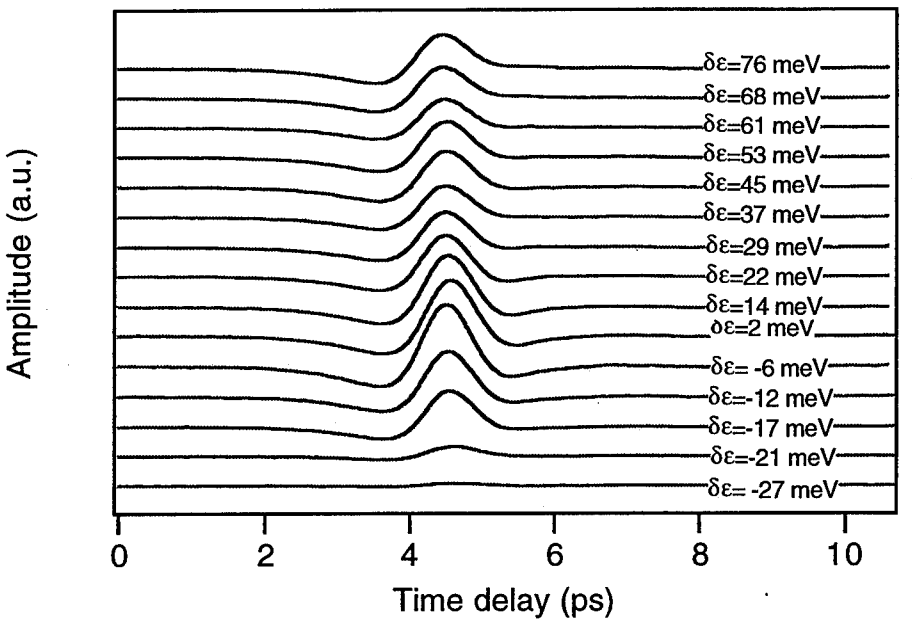

Figure 15

In conclusion, at a low dc bias field we have observed a dramatic waveform change of the THz radiation when the photon energy is tuned around the bandedge. This waveform change can be qualitatively explained in terms of a competition between the radiative contributions from both displacement and transport currents using a theory based on a fully quantum mechanical treatment of the transient photoconductive response of GaAs. At a high bias field, the transport current dominates, and no change of the THz waveform is observed.

D. Observation of Gunn Oscillation by triggering a vertical Gunn diode with femtosecond optical pulses:-

Optical sources with subpicosecond time duration are commonplace in high speed optoelectronics laboratories. The current challenge is to develop a reliable means of converting such ultrafast optical pulses into a comparable high-speed electrical transient. Recently, we have demonstrated a new method which will enable us to generate intense bursts of electrical oscillations in the THz region of the electromagnetic spectrum. This method is based on the idea of triggering Gunn oscillations [27] in a vertical Gunn diode with a femtosecond optical pulse. To do so, we designed a vertical transferred electron device (TED), e.g. a Gunn diode, with an intrinsic buffer layer between the active region and the cathode. The speed of a Gunn diode itself is normally determined by the length of the active region, and the upper limit is intrinsically set by the time carriers need to transfer from the L valley to the Γ valley which has been measured to be about 2 ps.

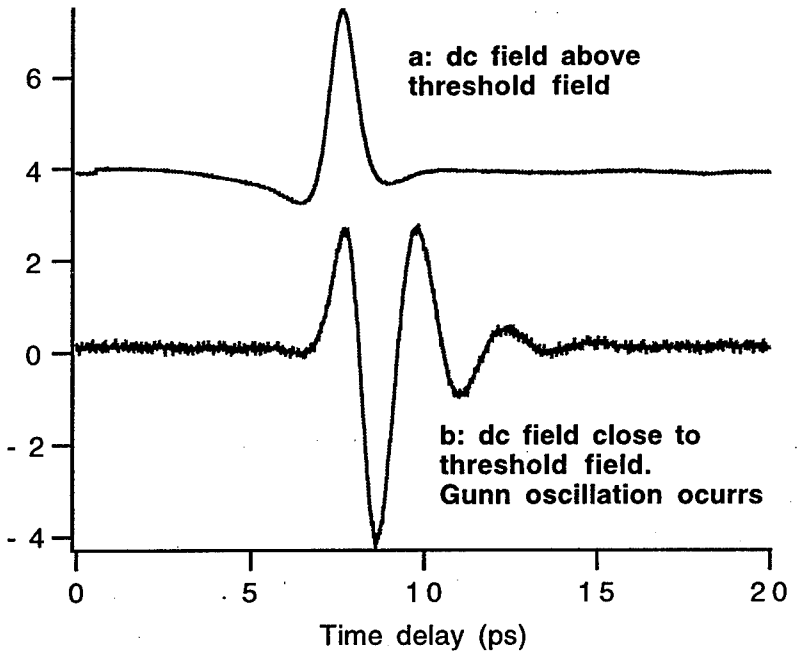

Figure 16

Initially, the vertical device is biased in such a way that the field in the active region is slightly below the threshold for Gunn oscillations to start. By choosing an appropriate femtosecond optical excitation source, we can inject a large number of photocarriers within the buffer layer. Therefore, the field of the active region is quickly switched above the threshold field, causing a burst of electrical oscillation. The duration of the oscillation is determined by the time required by photocarriers to sweep the buffer region, the carrier recombination time, etc. The coherent detection of this electrical burst can be achieved by measuring the radiated field in free space using a photoconductive dipole antenna.

Fig. 16 shows our preliminary results. The detected signal is composed of two contributions, one is the broadband signal caused by the fast initial rise of the photocurrent in the buffer region, the other is the narrow band oscillatory contribution due to the Gunn effect in the active region. When the bias field is much higher than the threshold, no Gunn oscillation is observed as shown in fig. 16a, while in the case where the field is close to the threshold voltage, an oscillation is observed as shown in fig. 16b. In the experiment described above, the Gunn diode could be replaced with a resonant tunneling diode (RTD), an IMPATT, or any other similar device involving an intrinsic high speed process.

IV. Tunable Narrowband THz Radiation

In spite of the abundance of optical transitions between energy states of various systems such as rotational and vibrational levels of molecules, phonons, energy gaps in superconductors, etc., spectroscopy in the sub-millimeter wave region has traditionally lagged behind its

counterparts in other regions of the electromagnetic spectrum. This is primarily because of the lack of tunable bright sources and sensitive detectors [28]. This has particularly affected the study of nonlinear and transient phenomena in this region. Optical difference frequency mixing has been developed extensively as an efficient technique for generating and detecting tunable coherent FIR radiation. The frequency content of the nearly single-cycle freely propagating THz radiation produced by conventional methods which use broadband optical excitation extends out to a few THz. This implies that other than the inherent limitations imposed by the frequency response of the combination of the emitting photomixer and detector, and the optical bandwidth available, no direct control over the frequency content of the THz radiation generated is possible.

While these broadband techniques are powerful and well suited for many applications, certain important studies require either tunable narrowband THz radiation or detection. In particular, identification and characterization of weak nonlinear interactions, such as second harmonic generation in the THz region will benefit greatly from spectral control of narrowband radiation. To this end, we have demonstrated a novel method of both generating and coherently detecting freely propagating narrowband THz radiation tunable out to ~1 THz. We describe below, the basic concepts, our experimental results, and applications of our recent work on tunable, narrowband optoelectronic sources and detectors of free space THz radiation.

A. Chirped pulse beating:

Recently, we reported a novel modification of the existing technique of generating broadband free space THz from large-aperture photoconducting antennas by incorporating a simple frequency tuning scheme into it [29]. This scheme relies on the quasi-sinusoidal optical modulation obtained by beating two linearly chirped broadband optical pulses with a variable delay. The basic scheme for producing narrowband optical modulation at tunable THz frequencies is illustrated in fig. 17. A broadband transform-limited optical pulse is temporally stretched using a pair of parallel diffraction gratings so that its instantaneous carrier frequency is linearly swept in time across the output pulse duration. The chirped pulse is then split into two pulses by a 50/50 beamsplitter and one pulse is delayed by a variable interval τ with respect to the other using a Michelson interferometer arrangement. The two collinearly propagating pulses are then recombined in the optical mixer so that their spectra overlap in the time-domain. If these pulses are linearly chirped, then at each point in time their frequency content differs by a constant beat frequency f_0, which is directly proportional to the time delay τ and the amount of frequency chirp in the input pulse. Any square-law photomixer such as a photoconducting antenna or a nonlinear $\chi^{(2)}$ crystal can then convert this quasi-sinusoidal optical modulation into freely propagating pulses of narrowband THz radiation with a center frequency f_0, which can then be tuned simply by varying the delay τ.

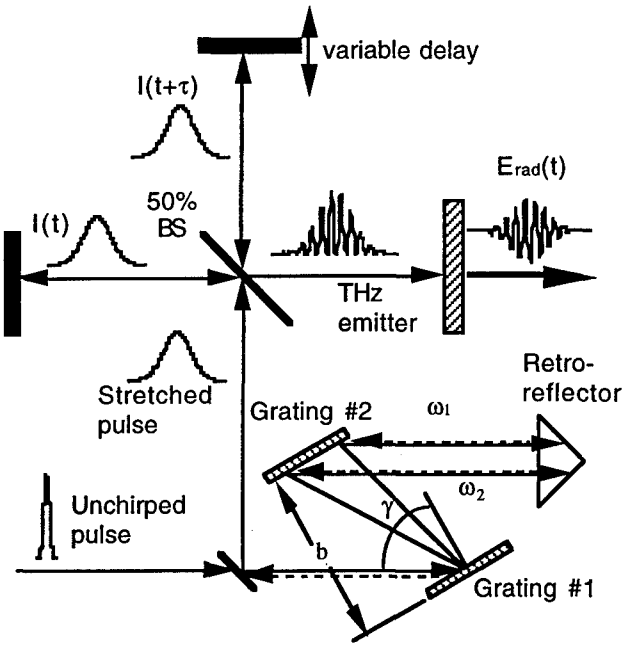

Figure 17

To illustrate the basic concept involved, we consider an optical pulse with a spectrum centered at w_0, with an amplitude A(t) and phase $\chi(t)$, whose electric field is given by $E_{in}(t) = A(t)\exp(-i\chi(t) - i\omega_0 t)$. When such a pulse propagates through a linear dispersive medium, it undergoes a frequency dependent phase modulation given by

$$\Phi(\omega) = \Phi(\omega_0) + \tau_0(\omega - \omega_0) + \frac{(\omega - \omega_0)^2}{2\mu} + \beta(\omega - \omega_0)^3 + \ldots \qquad (9)$$

Here, τ_0 is the group delay at ω_0, μ is the carrier frequency sweep rate, and β is the cubic phase modulation that becomes important in certain cases as discussed below. Our experimental scheme requires us to be able to introduce a controlled amount of linear chirp while keeping the quadratic (i.e. β) and higher order chirp sufficiently low. The phase modulated output pulse is then given by

$$E_{out}(t) = \frac{1}{2\pi}\int_{-\infty}^{\infty} d\omega e^{-i\omega t} e^{i\Phi(\omega)} \int_{-\infty}^{\infty} dt' e^{i(\omega-\omega_0)t'} A(t') e^{i\chi(t')} \qquad (10)$$

In order to be able to perform analytical calculations, we consider a transform-limited optical pulse with a Gaussian envelope of e^{-1} half width σ and a Gaussian spectrum centered at ω_0 (rad/s), i.e., $E_{in}(t) = E_0 \exp(-t^2/\sigma^2 - i\omega_0 t)$. The output of the Michelson interferometer through which the stretched Gaussian pulse is passed is then given by $I_{total}(t) = \left|E_{out}(t + \tau/2) + E_{out}(t - \tau/2)\right|^2$ where τ is the delay between the two arms. The output intensity can be written as

$$I_{total}(t) = I^+(t) + I^-(t) + 2E_0^2\left(\frac{\sigma}{\sigma_n}\right) e^{-2t^2/\sigma_n^2} e^{-\tau^2/2\sigma_n^2} \cos\left[\frac{2t\tau}{\sigma_n \sigma} + \omega_0 \tau\right] \qquad (11)$$

where $\sigma_n = \sigma(1 + 4/\mu^2\sigma^4)^{1/2}$ is the stretched pulsewidth and $\sigma_n >> \sigma$. The first two terms in the above expression are the low frequency (dc) components of the total intensity given by

$I^{\pm}(t) = E_0^2(\sigma/\sigma_n)\exp\left[-2(t \pm \tau/2)^2/\sigma_n^2\right]$. They correspond to the slowly varying Gaussian envelope of $I_{total}(t)$. The last term is the cross term which contains the quasi-sinusoidal optical modulation at the beat frequency f_0 (Hz) which is given by

$$f_0(\tau,\mu) = \frac{\tau}{\pi\sigma_n\sigma} \cong \frac{\mu\tau}{2\pi} \tag{12}$$

As can be seen from the Fourier transform of $I_{total}(t)$, the bandwidth of the optical intensity modulation at f_0 is also proportional to the linear chirp rate μ. It is given by the optical bandwidth $\Delta\nu_{opt}$ divided by the pulse stretching ratio, i.e.,

$$\Delta f = \frac{\sqrt{8}}{2\pi\sigma_n} \cong \frac{\sqrt{2}\sigma\mu}{\pi} = \Delta\nu_{opt}\left(\frac{\sigma}{\sigma_n}\right) \tag{13}$$

Also, it should be noted that the cross term falls as $\exp\left(-\tau^2/2\sigma_n^2\right)$ with increasing the delay t, and this determines the tuning range of the beat frequency f_0 to be $\sqrt{2}/\sigma\pi$, which corresponds to the optical bandwidth of the input pulse.

There exist several techniques of introducing controlled amounts of linear frequency chirp in broadband optical pulses using angular dispersion of linear optical elements such as diffraction gratings, prisms, etc.. A compact table-top setup consisting of a pair of parallel diffraction gratings can be used to stretch ~100 fs optical pulses by factors ranging from 10 to 20,000. The negative group velocity dispersion (GVD) introduced by such a grating pair is given by [30]

$$\frac{1}{\mu} = \left.\frac{\partial^2\Phi(\omega)}{\partial\omega^2}\right|_{\omega=\omega_0} = \frac{-4\pi^2 cb}{\omega_0^3 d^2}\left\{1-\left[\left(\frac{2\pi c}{\omega_0 d}\right)-\sin\gamma\right]^2\right\}^{-3/2} \tag{14}$$

where d is the grating constant, g is the angle of incidence of the input beam, and b is the perpendicular separation between the gratings which can be adjusted for the required pulse stretching factor (fig. 17). This simple low-loss method of introducing large linear chirps has inherent limitations in that higher order dispersion terms become significant for large input fractional bandwidths and pulse stretching factors. The cubic phase term in eqn. (9) for the grating pair has been shown to be [31]

$$\beta = \frac{1}{6}\left.\left(\frac{\partial^3\Phi(\omega)}{\partial\omega^3}\right)\right|_{\omega=\omega_0} = \frac{1}{2\mu\omega_0}\left[\frac{1+(2\pi c/\omega_0 d)\sin\gamma-\sin^2\gamma}{1-\left((2\pi c/\omega_0 d)-\sin\gamma\right)^2}\right] \tag{15}$$

The analytical evaluation of the integral in eqn. (10) considering terms up to the third order in eqn. (9) for $\Phi(\omega)$ for a Gaussian pulse input gives Airy functions and is impossible for arbitrary pulse shapes and higher than cubic phase terms. We have numerically evaluated eqn. (10) using discrete Fourier transforms of the optical electric field. The effect of higher order dispersion on the output of the chirped pulse beating process is to broaden the spectral width of the intensity modulation at the beat frequency f_0 and to reduce the effective tuning range to a fraction of the input optical bandwidth.

1. Optical Cross-correlation measurements:- We have experimentally verified the optical intensity modulation produced by beating chirped pulses with a variable delay using standard second harmonic generation (SHG) based optical cross-correlation techniques [32]. In our experiments, we used ~160 fs (FWHM) pulses at 800 nm ($\Delta\lambda_{FWHM}$ ~8.3 nm) at a 76 MHz repetition rate from a self-modelocked Ti:sapphire laser as the input to our pulse stretcher. The stretcher consisted of two parallel diffraction gratings (1800 l/mm) which were double-passed to produce pulses with an FWHM ranging from 20 to 200 ps. After passing through the Michelson interferometer (fig. 17) the stretched pulse was cross-correlated with the output of the Ti:sapphire laser.

We performed background-free intensity cross-correlation measurements using non-collinear phase-matched SHG. We used a 0.4 mm thick type I KDP crystal in our experiments. Fig. 18(a) shows the results of a typical cross-correlation measurement for a delay τ = 3.0 ps between the chirped pulses. The center frequency f_0, the FWHM bandwidth Δf, and the relative amplitudes at f_0 of the intensity modulation produced by chirped pulse beating for various delays τ were obtained from numerical Fourier transforms of the recorded waveforms. Fig. 18(b) shows the variation of f_0 and Δf with the delay t and fig. 18(c) shows that of the relative amplitudes I_{max} of the peak of the intensity modulation spectra at f_0.

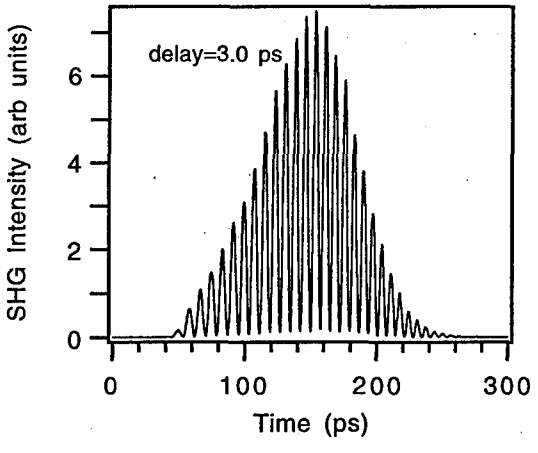

Figure 18(a)

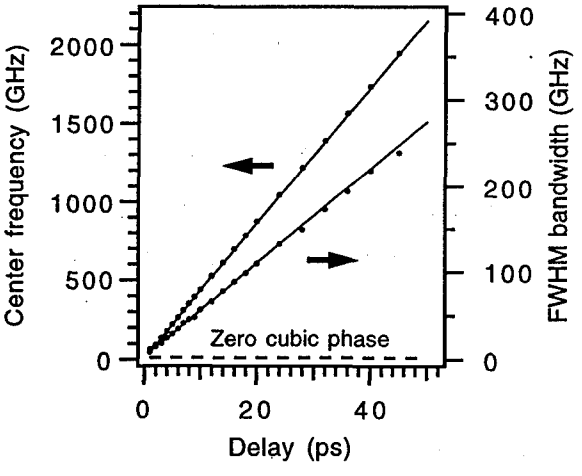

Figure 18(b)

Numerical simulations using discrete Fourier transforms (DFT) were carried out to obtain intensity modulation waveforms produced by beating chirped pulses with both quadratic and cubic phase modulation produced by the diffraction gratings. The slope of the experimental tuning curve (f_0 vs.τ) was used to obtain a value of the linear chirp factor μ =2.72x10^{23} rad^2/s^2 from eqn. (5). Eqn. (6) for the quadratic phase modulation of our grating pair then gave an effective separation of b =18.3 cm. The measured value of b =18.8 cm implies that the input to the grating-based dispersive line had a small amount of positive GVD as can be expected from propagation through various optics. We measured an autocorrelation width of ~225 fs for the output of the Ti:sapphire

oscillator while a cross-correlation measurement of the stretched pulse gave a width of ~93 ps. The above value of μ corresponds to a width ~90 ps for a linearly chirped Gaussian pulse with a 8.3 nm FWHM bandwidth at 800 nm.

Cubic and higher order phase modulation implies a variation in the instantaneous difference frequency f_0 between the two chirped pulses across the duration of the chirped pulse beating output, $I_{total}(\tau)$. Although the duration of the stretched pulse is not affected appreciably, this leads to a broadening of the intensity modulation spectrum which increases with the delay τ as can be seen from the fit to the Δf vs. t curve in fig. 18(b). However, the variation of the beat frequency f_0 with the delay τ remains unaffected.

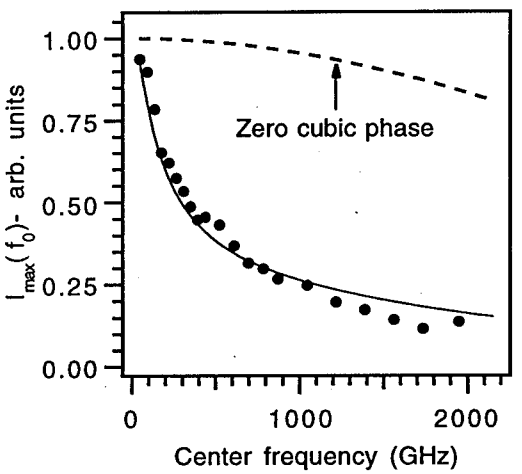

Figure 18(c)

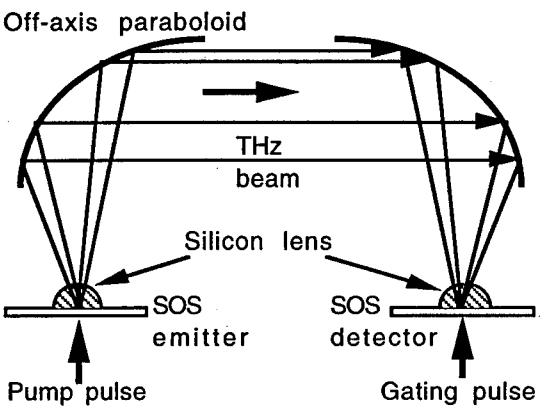

Figure 19(a)

The figure also shows the variation of Δf with τ in the absence of a cubic phase term in the grating dispersion equation which is in very good agreement with eqn. (5). Another deleterious effect of cubic phase modulation borne out by both the experimental data and the simulation is the decrease in the effective tuning range of the beat frequency f_0. As shown in fig. 18(c), the value of I_{max} at f_0 falls off much more rapidly with the delay τ in the presence of cubic phase and it no longer follows the $\exp(-\tau^2/2\sigma_n^2)$ trend as expected in the zero cubic phase case.

B. A tunable THz beam system using photoconducting dipole antennas:-

As discussed above, photoconducting dipole antennas can act as broadband nonlinear photomixers to convert the narrowband intensity modulation produced by chirped pulse beating into tunable narrowband FIR radiation. Since the radiated field is directly proportional to the instantaneous optical intensity, we expect that the frequency content of the THz produced to follow that of the incident optical intensity $I_{total}(t)$. The experimental setup used to generate and coherently detect this tunable THz radiation shown in fig. 19(a) is similar to the THz time-domain spectroscopy system of Grischkowsky *et al.*. [3]. It consists of identical 100 μm receiving and transmitting antennas fabricated on ion-implanted silicon-on-sapphire (SOS). In the first set of

experiments, the photoconductive gap of the transmitting antenna is gated by the output of the Michelson interferometer used to mix chirped optical pulses (λ_0 =800 nm, $\Delta\lambda$ ~8.3 nm), as described above. This dipole antenna emits narrowband THz radiation into free space. This radiated field is then coherently detected after propagation through ~40 cm of air by an identical receiving dipole antenna whose active gap is gated by the output of the Ti:sapphire oscillator.

Fig. 19(b) shows a typical time-resolved measurement of the radiated field obtained from a 100 μm dipole generator-detector combination where both the THz emitter and the detector were excited by ~160 fs pulses from the Ti:sapphire oscillator. Fig. 19(c) shows a similar measurement obtained for the case of narrowband THz produced by chirped pulse beating in the emitter. In both the cases, the average optical power in the pump and the probe beams and the bias on the emitter were identical. The impulse response of the overall THz beam system is given by the Fourier transform of the broadband THz field of fig. 19(b). The high-frequency part of this response is limited primarily by the finite risetime of the photocurrent in the emitter, the antenna response, which drops when the wavelength of the emitted radiation becomes comparable to the length of the antenna, and the non-ideal imaging properties of the THz optics [3]. This limits the overall tuning range achievable by the present system to ~0.06-0.8 THz. Another factor limiting the signal-to-noise ratio in our experiments is the fact that the peak signal falls by a factor on the order of the pulse stretching ratio (σ_n/σ ~800 in our case), as can be seen from figs. 19(b) and 19(c).

The center frequency f_0 and the FWHM bandwidth Δf of the narrowband THz were obtained from Gaussian fits to the Fourier transforms of the waveforms recorded using the above setup for various delays τ between the chirped pulses incident on the dipole emitter.

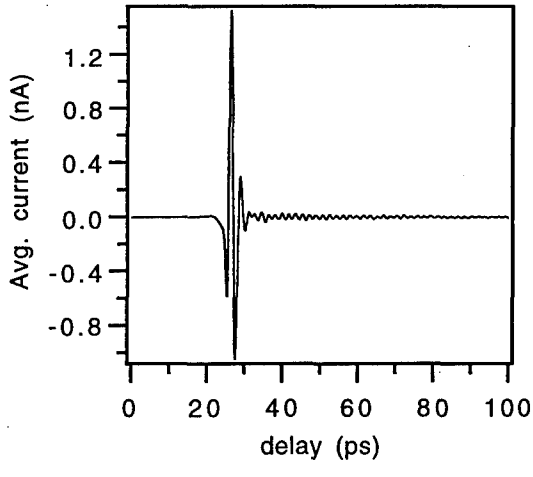

Figure 19(b)

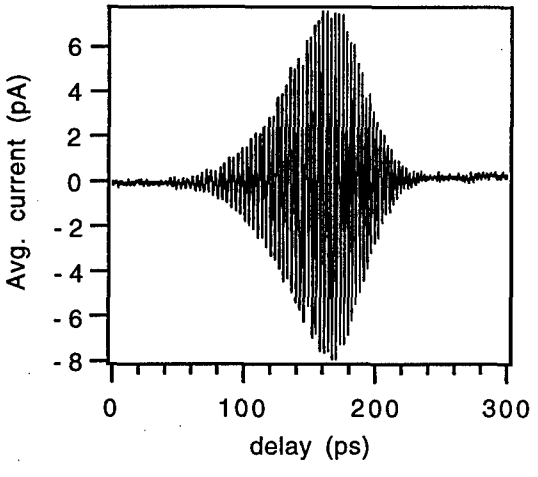

Figure 19(c)

Numerical fits to the observed variation of both f_0 and Δf with τ were calculated for the case of chirped pulse beating in the presence of cubic phase modulation in the dispersive line. The values of the quadratic and cubic phase terms (μ and β) used for the numerical fits to this data were within 10% of those used for the SHG cross-correlation data in fig. 19(b). In order to ensure that our

emitter was not being saturated due to screening of the bias field by the injected carriers, we verified the linearity of the radiated field with the incident optical intensity [33].

C. Tunable THz detectors:-

In the second set of experiments, the frequency tunability was incorporated into the receiving antenna instead of the emitter. This was accomplished by using the narrowband intensity modulation produced by chirp pulse beating to modulate the conductivity of the detecting dipole. The emitter was pumped by femtosecond pulses from the Ti:sapphire oscillator while the detector was gated by the output of the Michelson interferometer described above. The average photocurrent in the detector is given by the convolution over time of the THz field and its time-dependent conductivity. Hence, the overall system response at any THz frequency ω can be written in terms of the average photocurrent recorded by the detector as

$$J_{avg}(\omega) = I_{pump}(\omega)H_{pc}(\omega)H_{THz}(\omega)H^{*}_{pc}(\omega)I^{*}_{probe}(\omega) \qquad (16)$$

where $H_{pc}(\omega)$ is the photocurrent response function of both the emitter and the detector (which includes the THz optical system response) [3]. By reversing the roles of $I_{pump}(\omega)$ and $I_{probe}(\omega)$ in the THz time-domain spectroscopy setup used in the previous set of experiments, we now have a coherent narrowband detector whose tunability is limited by its photoconductive response $H_{pc}(\omega)$. It should be noted that this scheme should work equally well for an asymmetric system where the emitter and the detector have different impulse responses $H(\omega)$.

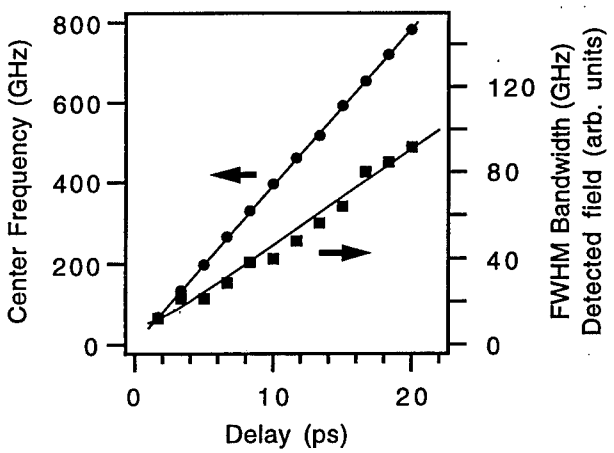

Figure 20(a)

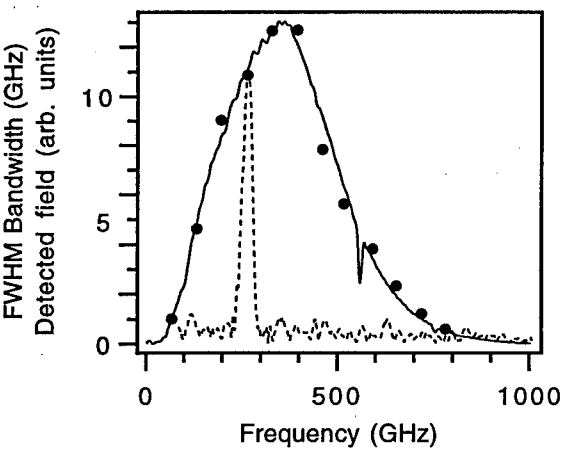

Figure 20(b)

The results of the time-resolved measurements using the tunable narrowband detector are identical to those obtained with a broadband detector (fig. 19(c)). Here again, as shown in fig. 20(a), the center frequency and bandwidth of the detected portion of the broadband THz spectrum radiated from the dipole emitter show the expected variation with the delay τ between the two chirped pulses gating the detector. Fig. 20(b) shows the relative amplitudes of the narrowband THz spectra detected by our tunable detector at various values of the center frequency (delay τ), along with the amplitude spectrum of the detected waveform (dotted line). Since the average probe

power remains fixed, we expect this narrowband detector frequency response to be a product of the variation of $I_{max}(f_0)$ shown in fig. 18(c) and the overall THz system response obtained from the Fourier transform of fig. 19(b). We have obtained reasonable agreement between our numerical calculations of this modified THz system response and our narrowband THz data both for the tunable emitter and tunable detector (fig. 20(b)).

Thus, we have a complete characterization of the frequency response of our tunable narrowband THz beam system based on chirped pulse beating in either the emitting or detecting dipole antennas. This system can now be used for narrowband time-domain spectroscopy over a wide frequency range in the THz region. It should be noted that the frequency resolution of this technique is the same as that of conventional Fourier transform spectroscopy, as they are both based on a scanning delay line whose resolution is determined by the reciprocal of the total time scan. This technique may be particularly appropriate to nonlinear spectroscopy and the time-domain study of nonlinear interactions in the FIR, since the emitted and the detected frequencies need not be the same.

A less fundamental limitation is the influence of cubic and higher order phase terms introduced by the diffraction gratings into the broadband input pulse. It has been demonstrated that a pair of prisms can be used to compensate for the cubic phase distortion produced by the diffraction gratings [34], so that improvements to the phase characteristics of the stretched optical pulse are clearly possible.

D. Generation of intense tunable THz from photoconducting antennas:-

We have demonstrated that large-aperture photoconducting antennas, where the linear dimension of the illuminated area is much larger than the center wavelength of the radiated field, have made it possible to produce optically steerable diffraction-limited beams of THz radiation. Further, due to their size, large-aperture antennas can sustain very high optical pulse energies and high bias fields, and are hence, ideally suited to scale up the peak power of the free space THz pulses without loss of THz bandwidth. The availability of such high energy far-infrared pulses synchronized with intense subpicosecond optical pulses from table-top amplifiers has enabled numerous time-resolved optical pump and THz probe measurements such as the study of relaxation dynamics of photoexcited carriers in GaAs and InP. However, it is now well known that the radiated fields from these broadband emitters saturate with increasing optical fluence due to the screening of the bias field by the injected carriers [33, 35].

For all our high optical fluence experiments, we have constructed a Ti:sapphire regenerative amplifier which is seeded by the self-modelocked Ti:sapphire oscillator described above and pumped by a frequency-doubled Q-switched Nd:YLF laser. This system, based on the concept of chirped pulse amplification to avoid deleterious nonlinear effects in the gain medium, is capable of producing 1 mJ, 150 fs pulses (corresponding to peak power > 5 GW) at 1 kHz. We have

explored the physics of saturation mechanisms in photoconducting antennas made up of various semiconductors by studying their behavior under such intense broadband and tunable narrowband optical excitation. We have recently shown that the use of stretched optical pulses in conjunction with such large aperture antennas can enable the achievement of higher optical-to-electrical conversion efficiencies within a given FIR bandwidth. This arises from the possibility of utilizing much higher optical fluences without deleterious saturation effects due to the bias field limited boundary conditions at the surface of the THz emitter.

Extensive numerical simulations of the saturation in planar photoconducting antennas using a simple model for the radiated field from a time-varying photocurrent [36] have shown that the spectral brightness of the narrowband emitters can exceed that of broadband emitters by factors as high as 200. The degree of enhancement over passive filtering of broadband signal is predicted to increase with decreasing carrier lifetime (photocurrent relaxation time). The results of the experiments performed with both large aperture and dipole antennas have demonstrated the possibility of working in this saturation regime. The observation that the peak THz signals obtained for a given optical pulse energy do not scale with the pulse stretching ratio as expected from a simple first order calculation, is a clear indication of the advantage of using narrowband emitters. Our technique provides an approach uniquely suited to the generation of pulses of intense narrowband THz radiation tunable over a wide range of frequencies optically synchronized with very intense broadband optical sources. This capability can be exploited to probe FIR excitations of surfaces and interfaces using nonlinear spectroscopic techniques such as sum-frequency generation. In the area of far-infrared nonlinear optics, various methods of harmonic generation can be readily explored with our technique.

E. Tunable far-infrared radiation from difference-frequency generation in lithium niobate:-

Optical difference frequency generation (DFG) using broadband optical excitation of nonlinear dielectric crystals such as $LiNbO_3$ has been demonstrated as a powerful technique to generate coherent free space FIR radiation [28, 37]. The frequency bandwidth of the THz radiation generated by optical rectification in such nonlinear crystals is limited, in principle, only by the bandwidth of the femtosecond optical excitation. However, as discussed in the previous sections, broadband phase matching is difficult to achieve due to the high FIR dispersion in $LiNbO_3$. We may turn this property to an advantage by using this frequency-selective process of phase matching [38] to control the spectral content of the THz radiation produced.

We have used type II phase matched difference frequency mixing in $LiNbO_3$ to generate narrowband THz radiation with ~150 fs pulses at 800 nm from a self-modelocked Ti:sapphire laser. The FIR refractive indexes and absorption coefficients were measured by THz time-domain spectroscopy. These measurements were applied to calculate frequency-dependent phase matching

curves from 0.1 to 1.0 THz. Using these data, we have obtained FIR radiation tunable from 0.3 to 0.7 THz with a bandwidth of ~12 GHz. The measured THz bandwidths agreed well with the dispersion-limited bandwidths calculated from the experimental dispersion data for $LiNbO_3$. Fig. 21 shows the observed THz field from a 5 mm thick $LiNbO_3$ cut at 15° off the c-axis detected using a 100 μm SOS dipole detector. The detected field spectrum (fig. 21b) shows both the forward and the backward phase-matched DFG signals generated. The same can be seen in the temporal waveform (fig. 21a).

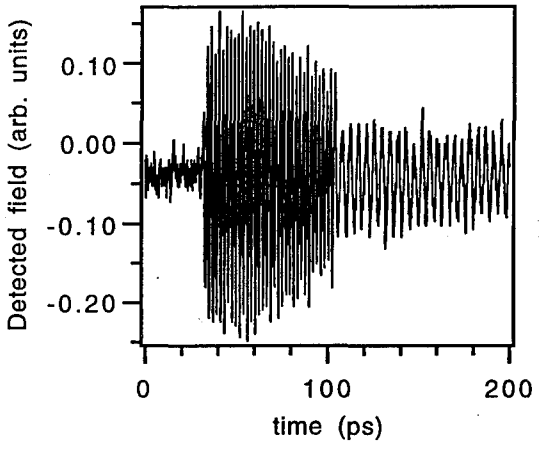

Figure 21a

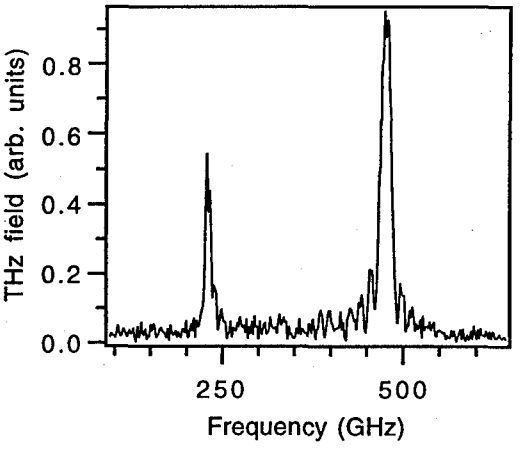

Figure 21b

We believe that the application of broadband chirped pulses will enable us to scale this narrowband THz field to greater intensities than those possible with femtosecond pulses. This expectation is based on the possibility of going up to higher optical fluences on the nonlinear crystal without causing optical damage when stretched pulses are employed. By using nonlinear media such as $LiNbO_3$ and organic crystals such as DAST, we also hope to extend the tuning range of our narrowband THz system to the optical bandwidths available.

V. Ultra-broadband THz Radiation

In this section, we review recent progress in our laboratory on the generation and detection of freely propagating THz radiation by means of second-order nonlinear effects. As discussed in the preceding sections , remarkable progress has been made in the development of spectroscopic capabilities for coherent THz measurements. Much of the work reported to date relies on the use of photoconductive elements both as emitters and detectors [3, 39]. While these devices are highly optimized in many respects, there are fundamental limitations in their frequency response associated with the natural time constants for carrier dynamics. The ready availability of extremely short laser pulses suggests the potential for extending the bandwidth of coherent spectroscopy to significantly higher frequencies. For example, a 10-fs transform-limited laser pulse at $\lambda_0 = 800$ nm has a bandwidth of 44 THz or roughly 1500 cm^{-1}. The use of materials with an instantaneous

optical response, such as the non-resonant electronic second-order nonlinear susceptibility $\chi^{(2)}$, may permit this enormous bandwidth to be captured both for the generation and detection of ultrafast electromagnetic transients.

A. Generation of THz radiation from poled polymers:-

In recent years, terahertz radiation has been generated from a variety of nonlinear optical materials [40-42]. Many of these materials exhibit a high degree of dispersion, corresponding to small coherence lengths for difference frequency mixing, and high absorption. This limits the total conversion efficiency. Polymeric media offer many attractive properties for far infrared generation. In addition to being relatively low loss, low dispersion materials, they are readily processable, can be poled to induce non-centrosymmetry, and may possess nonlinear coefficients greater than that of lithium niobate. As discussed below, we have generated THz radiation from an organic poled polymer. We believe that these materials have potential both for very intense FIR emission and for extending the spectral range well beyond that attainable using photoconductors.

We used a conventional pump-probe experimental setup for generating and detecting the THz radiation [41] with a poled polymer used as the emitter. The polymer consisted of a copolymer of 4-N-ethyl-N-(2-methacryloxyethyl)amine-4'-nitro-azobenzene (MA1) and methyl methacrylate (MMA) obtained from AlliedSignal [43]. In the experiments, a free-standing 16 mm thick film, with dipolar alignment perpendicular to the surface was used [44]. The polar axis (z') of the uniaxial nonlinear medium was determined by the direction of the poling field. The optical excitation pulses were generated by a mode-locked Ti:sapphire laser operating at 800 nm. An s- or p-polarized pump beam, with average power up to 600 mW and spot diameter of 1 mm at the sample, was used to pump the polymer film. The generated THz radiation was focused onto a 100 μm radiation damaged silicon-on-sapphire dipole detector, aligned to detect p-polarized radiation.

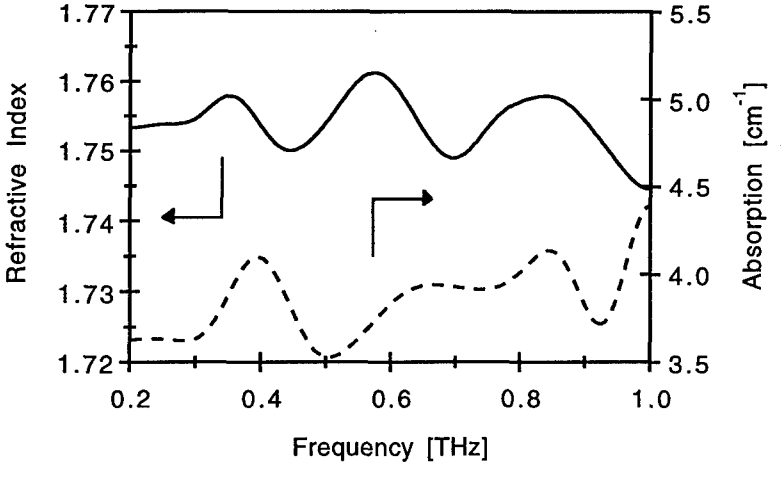

Figure 22

We first measured the refractive index and absorption of the MA1:MMA polymer film. This was accomplished by THz time-domain spectroscopy [3] using a bare <100> GaAs wafer as the emitter. Fig. 22 shows the resulting refractive index and power absorption from 0.2 to 1.0 THz. As can be seen, the absorption is very weak over the entire spectral range and the refractive index is essentially flat. We believe that the observed oscillations are artifacts due to diffraction effects caused by the aperture and the finite Fourier transforms taken in the data analysis. The coherence length, ℓ_c, for difference frequency mixing is given by

$$\ell_c = \frac{\pi c}{\omega_{THz}\left| n_{opt} - \lambda_{opt}\left.\frac{dn_{opt}}{d\lambda}\right|_{\lambda_{opt}} - n_{THz}\right|} \qquad (17)$$

where c is the speed of light, n_t and n_{opt} are the THz and optical frequency refractive indexes, respectively, ω_{THz} is the far-infrared frequency, λ_{opt} is the optical wavelength, and $dn_{opt}/d\lambda$ is a measure of the optical dispersion. The coherence length is >1 mm for all FIR frequencies below 10 THz. For comparison, the corresponding coherence lengths in $LiNbO_3$ are nearly 200 times smaller. If we assume uniform generation throughout a 1 mm thick polymer with an absorption coefficient of a ~ 4 cm^{-1}, only 10% of the far infrared radiation would be reabsorbed at frequencies between 0.2 and 1.0 THz. Thus, we should be able to effectively exploit the large coherence lengths of these polymeric materials.

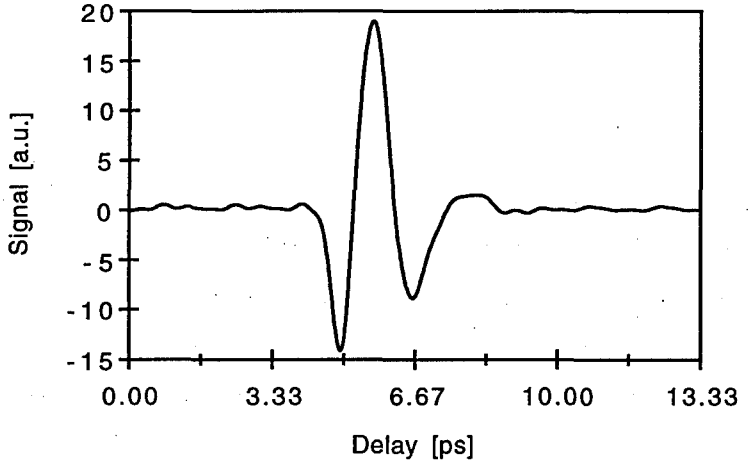

Figure 23

The low frequency electro-optic coefficient of our 16 μm thick sample was r_{33} ~ 11 pm/V [43, 44]. The peak signal from the polymer sample, shown in fig. 23, was roughly a factor of 4 smaller than the maximum signal obtained from a $LiNbO_3$ crystal with a thickness of 1 mm. The relatively small difference in the peak THz signals observed between the two materials is due to the short coherence lengths and large THz refractive index of $LiNbO_3$, corresponding to greater

Fresnel reflection coefficients. Note that the intrinsic nonlinear response (r_{33} = 31 pm/V) of $LiNbO_3$ is comparable to that of our polymer.

In order to verify that the THz signal is indeed due to optical rectification, we measured the p-polarized THz radiation as a function of incidence angle and pump polarization. The experimental data obtained from the 16 μm thick sample is shown in fig. 23 for p- and s-polarized pump beams for angles of incidence θ ranging from 0° to 60°. The radiated electric field is proportional $\omega^2 P_{NL}$, where ω is the far infrared frequency and P_{NL} is the effective nonlinear polarization. For an s-polarized pump beam and a p-polarized THz beam, the radiated field is proportional to $P_{NL(pss)} \sim A[d_{31}\sin\theta_m]E_x E_x^*$.

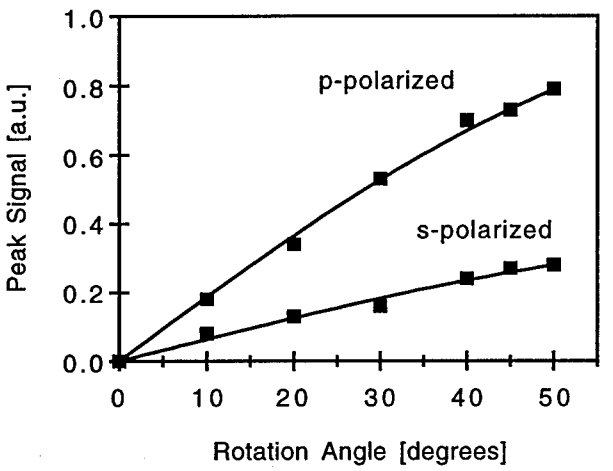

Figure 24

Similarly, for a p-polarized pump beam and a p-polarized THz beam, the radiated field is proportional to $P_{NL(ppp)} \sim A'[(3d_{33}+3d_{31})\sin\theta_m + (3d_{31}-d_{33})\sin(3\theta_m)]\ E_z E_z^*/4$, where A and A' are constants and θ_m (= $\sin^{-1}[\sin\theta / n_{opt}]$) is the propagation angle in the polymer medium. The experimental data shown in fig. 24 is corrected for the angularly dependent transmission coefficients and effective pathlength. We simultaneously fit to the two nonlinear polarization expressions assuming A=A'. The resulting best-fit yields a value of d_{31}/d_{33} = 0.34. A simple thermodynamic model for poled polymers [45] yields a calculated value of d_{31}/d_{33} = 0.30 [44].

In future experiments, we hope to demonstrate scaling of the THz radiation to increasingly high intensities. This may be achieved using polymers with of millimeter thickness, as argued above. Use of amplified laser pulses should further enhance the THz radiation intensity. Unlike photoconductively gated devices, the radiated electric field from polymers is expected to vary linearly with the pump intensity up to the damage threshold of the medium. We also intend to verify the capabilities of these materials to support optical rectification of laser pulses as short as 10 fs, with corresponding bandwidths of 10's of THz.

B. Coherent detection of free space THz radiation by electro-optic sampling:-

To date, the only broadly applicable technique to coherently detect THz radiation requires the use of synchronously gated photoconducting dipole detectors [3, 39]. While these detectors exhibit excellent sensitivity, it is difficult to calibrate the measured electric field. Additionally, there is a strong speed versus sensitivity trade-off which is determined by the photoconductive response and antenna dimensions [3]. While electro-optic sampling [46] has been used extensively to study ultrafast electrical pulses, these applications have been primarily limited to transmission line and circuit characterization. The significant advantages of this technique are the capability of detection that is limited only by the optical bandwidth and the ability to calibrate the detected electric field. The former is especially true with the use of poled polymers, where the material response time is negligible [43, 47].

Electro-optic sampling has recently been demonstrated as a technique for the coherent detection of *freely propagating* sub-millimeter wave radiation [48, 49]. In our experiments described below, the emitter and detector are physically separated by a large distance. The electro-optic sampling is performed in a poled polymer that is similar to that discussed in the previous section. We fabricated the electro-optic sampling element (EOSE), shown schematically in fig. 25, on an R-plane sapphire substrate.

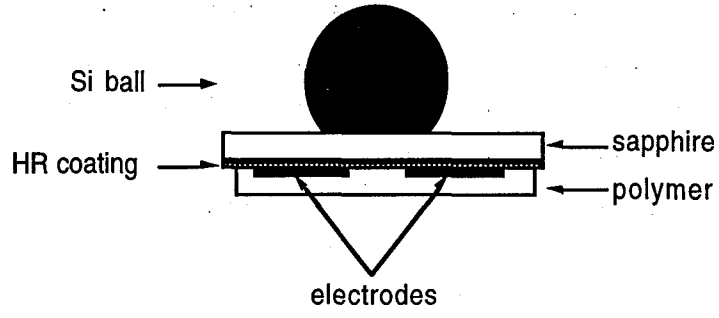

Figure 25

A high reflectivity dielectric coating centered at 800 nm was first evaporated onto one side of the substrate. Two coplanar 5 mm x 5 mm x 2000 Å thick aluminum pads separated by 50 μm, used for poling, were then photolithographically defined onto the coating. A 10 μm thick film of the nonlinear copolymer was then cast from solution, baked at 130° C for 3 hours in air, and poled. A hyperhemispherical silicon lens was attached to the sapphire substrate to focus the THz radiation into the electrode gap.

The experimental setup used for generating and detecting THz radiation is shown in fig. 26. A mode-locked Ti:sapphire laser operating at 800 nm with energy of 10 nJ and 160 fs pulse duration was used to generate and detect the transient sub-millimeter wave pulses. A p-polarized pump beam, chopped at 95 kHz, was used to drive a large aperture photoconducting antenna. The emitter was biased with voltages ranging from +300 V to -300 V and oriented so that the resulting

THz radiation was p-polarized. A pair of off-axis paraboloidal mirrors was used to collimate and focus the THz radiation into the EOSE. The total separation between the emitter and detector was 60 cm.

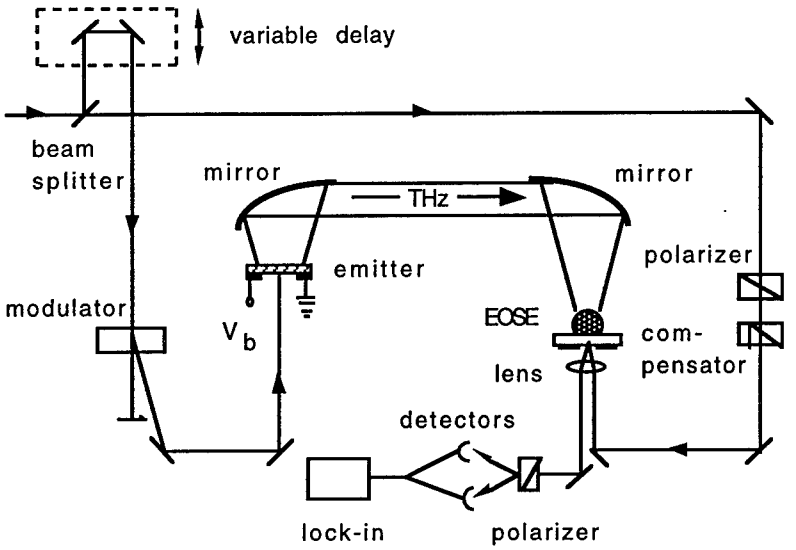

Figure 26

The detection system employed a crossed polarizer arrangement with differential detection [46]. The 5 mW probe beam was optically biased at its quarter wave point by a Soleil-Babinet compensator and focused into the electrode gap of the EOSE. The c-axis of the poled polymer was parallel to the incoming p-polarized THz radiation. The reflected probe beam, split by the Wollaston prism, generated a quiescent current of approximately 1 mA in each detector. The differential signal was amplified, digitized and averaged using a computerized data acquisition system.

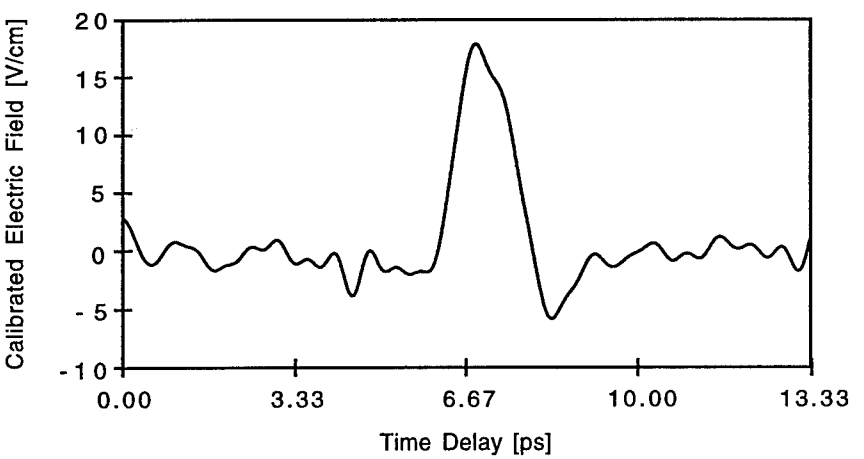

Figure 27

The temporal response of the system with an antenna bias of 300 V is shown in fig. 27. We calibrated the THz response of the EOSE by applying a DC bias across the 50 μm electrode gap. Such a calibration requires that we neglect the difference in field distributions between the

diffracted THz field and the fringing applied voltage. We also neglect the dispersion of the electro-optic coefficients. The latter assumption reasonable since the optical nonlinearity is electronic in nature, as shown by comparing electro-optic and second harmonic generation measurements [47]. The peak detected field was found to be ~18 V/cm with a noise floor of 2.9 (V/cm) / $\sqrt{\text{Hz}}$.

The observed DC electro-optic coefficient r_{33} was determined to be 11 pm/V, corresponding to a value of E_π, the field needed to cause a π phase retardation, of 12 MV/cm. In the shot noise limit, we found that the minimum detectable field for our detection system is

$$E_{min} = E_\pi \sqrt{\frac{q}{2I_o}} \frac{(V/cm)}{\sqrt{Hz}}. \qquad (18)$$

Thus, for a quiescent current of 1 mA and 1 Hz bandwidth, the minimum detectable field is 100 (mV/cm)/$\sqrt{\text{Hz}}$. Our present detection noise floor is nearly 29 dB above the shot noise limit and appears to be dominated by excess laser noise. We are currently working to reduce the system noise.

In the far field, the radiated THz electric field is expected to have a bipolar shape, such that total time integral is zero [39, 49]. The observed shape of the detected waveform in fig. 27, however, is unipolar. This effect is the result of the perturbation of the applied THz field induced by the metal electrodes in the EOSE. A similar effect was observed in the first description of photoconducting Hertzian dipole detectors [50]. We modeled the influence of the electrodes by considering classical electromagnetic diffraction through a 2-dimensional conducting screen with a narrow slit [50]. Such a model is appropriate since the electrodes are significantly larger than the wavelengths of interest. To first approximation, the diffracted field (and corresponding electrode voltage) is proportional to the time integral ($\omega^{-1}E(\omega)$) of the incident field. This is equivalent to the charging of the gap capacitance by the incident THz radiation. An approximate expression for the voltage across the slit can be written as [50]

$$v_s(t) = \frac{1}{Z_o C_s} \int_{-\infty}^{t} dt' E_i(t') \qquad (19)$$

where Z_o is the characteristic impedance of the medium and C_s , which has a weak frequency dependence, is the static capacitance of the electrode structure per unit length.

We demonstrate the integrating nature of the EOSE by comparison with a 100 μm Hertzian dipole detector that has been shown to preserve the bipolar nature of the incident electric field waveform [3]. Fig. 28a shows the detected waveform with the dipole detector substituted for the EOSE with all other experimental parameters unchanged. As expected, this waveform is bipolar. The time integral of this signal is shown in fig. 28b. While the waveform shapes of figs. 27 and 28b are very similar, the FWHM time of the former signal is smaller. To understand this, we consider the response time of the EOSE, neglecting its integrating nature. The detection response time of the sampling system is given by $\tau_s = \sqrt{\tau_{pw}^2 + \tau_{it}^2 + \tau_{mr}^2}$. Here, τ_{pw} is the FWHM optical

pulsewidth of the probe beam and is equal to 160 fs. The interaction time of the optical pulse through the nonlinear medium $\tau_{it} = 2n\ell/c$ is 110 fs and the material response time τ_{mr} is < 10 fs [52]. Thus, the overall FWHM detection response time τ_s < 200 fs, which is smaller than that of our dipole detector.

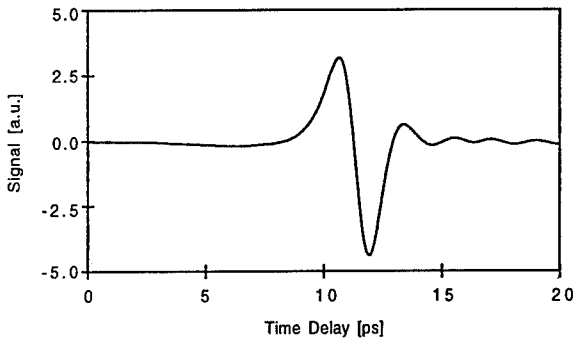

Figure 28a

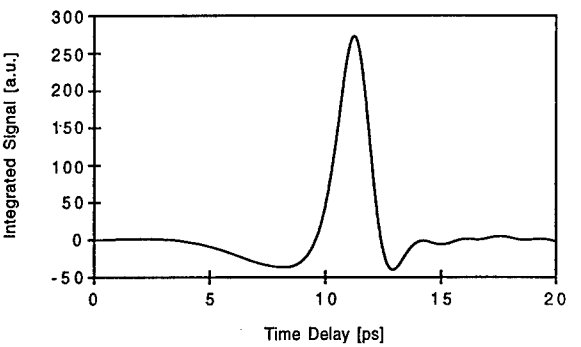

Figure 28b

It should be possible to modify the sampling element so that the incident field is not diffracted. This can be accomplished by removing the electrodes after poling or by using an appropriate organic single crystal. In addition to reducing laser noise, improvement in the detection sensitivity should be possible by performing the experiment in a transmission geometry. In this geometry, the THz field would again be normally incident on the EOSE. The probe beam, however, would be incident at the phase velocity matching angle. This angle is relatively small in polymers due to the low refractive index dispersion [44]. The probe beam, therefore, copropagates with the THz beam allowing for longer interaction lengths. These ideas are currently being investigated.

C. Ultra-broadband Coherent Terahertz Spectroscopy Using Optical Rectification and Electro-optic Sampling:-

In recent years, remarkable progress has been made in the development of spectroscopic capabilities for coherent terahertz (THz) measurements. A key ingredient to these advances is the development of ultra-broadband coherent sources and detectors of THz radiation. Much of the work reported to date relies on the use of photoconductive elements both as emitters and detectors. While these devices are highly optimized in many respects, there are fundamental limitations in their frequency response associated with the natural time constants for carrier dynamics. The ready availability of laser pulses with durations of ~10 fs suggests the potential for extending the bandwidth of coherent spectroscopy to significantly higher frequencies. By using materials with an instantaneous optical response for both emission and detection, it may be possible to capture much of this enormous bandwidth. Thus, the use of materials with non-resonant second-order optical nonlinearities is optimally suited for these applications.

The combination of broadband optical rectification and electro-optic sampling have been demonstrated in $\chi^{(2)}$ media [53, 54]. In order to enhance the sensitivity, longer interaction lengths are desirable, necessitating appropriate consideration of phase matching constraints. In our most recent work, we have addressed this issue of phase matching to allow for greater interaction between the optical and THz pulses in the nonlinear medium in order to enhance the efficiency of both the generation and detection processes [53]. We have demonstrated that dispersion in the optical refractive index may be used to obtain collinear, non-critical phase matching over a broad bandwidth in the THz. For a medium with dispersion at the optical frequencies, the phase matching condition for both difference-frequency mixing and electro-optic sampling can be written as

$$\frac{k(\omega_{THz})}{\omega_{THz}} \approx \left(\frac{\partial k}{\partial \omega}\right)_{opt} \qquad (20)$$

This relation implies that phase matching is achieved when the phase of the THz wave travels at the velocity of the optical pulse envelope (i.e., the optical group velocity, v_g). Optical [55] and THz dispersion [56] data indicate that sufficient group velocity dispersion exists within ZnTe to obtain phase matching at $f_{THz} \sim 2$ THz. The possibility of obtaining phase matching in this manner at a pump wavelength of 800 nm is illustrated in fig. 29 for ZnTe, the material used in our experimental investigations.

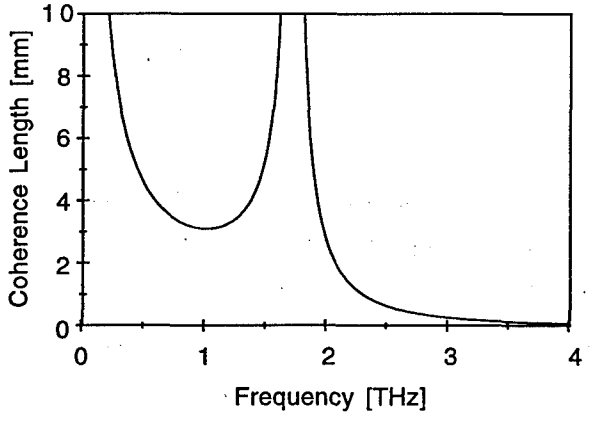

Figure 29

The coherence decreases because of dispersion in the THz refractive index, but remains large over a wide range of frequencies. Using optical rectification and electro-optic sampling in <110> ZnTe for the generation and coherent detection of freely propagating THz radiation, respectively, we have demonstrated spectral sensitivity beyond 3 THz [53].

A mode-locked Ti:sapphire laser producing 130 fs pulses at 800 nm with a 76 MHz repetition rate was used to generate and detect the FIR pulses. A 2 mm diameter pump beam, appropriately polarized in order to maximize the nonlinear response, was chopped and used to drive a 0.9 mm thick <110> ZnTe emitter at normal incidence. The THz electromagnetic transient

produced by optical rectification in the ZnTe crystal was imaged into an identical ZnTe crystal (the E-O sampling element) using two off-axis paraboloidal mirrors. The total separation between the emitter and detector was 50 cm. A pellicle beamsplitter was interposed in the THz beam line to allow for co-propagation of the optical probe and THz beams through the EOSE. The temporal waveform of the measured THz electric field is shown in fig. 30. The full width at half maximum (FWHM) pulsewidth is approximately 270 fs. The frequency response of this system is limited primarily by phase matching characteristics (the maximum frequency for obtaining a coherence length of at least 0.9 mm is ~2.5 THz). In addition to these limitations, the dispersion and absorption caused by the dominant low frequency resonance in ZnTe at 5.4 THz strongly attenuate the high frequency components [56].

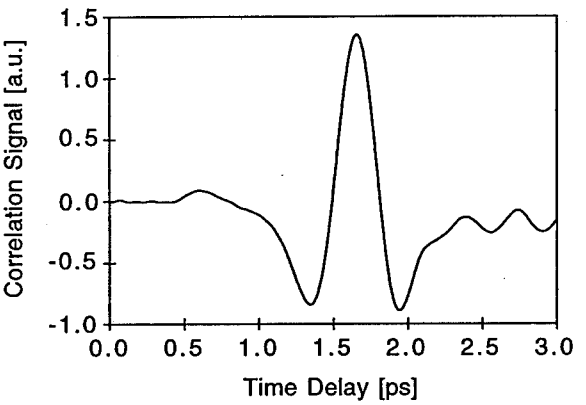

Figure 30

For a 0.9 mm thick ZnTe EOSE and shot-noise limited differential detection, photomodulation as small as ~5 x 10^{-8} may be detected (corresponding to a minimum detectable field of ~2 (mV/cm)/$\sqrt{\text{Hz}}$). Such a significant improvement in sensitivity of the EOSE as compared to the earlier work using poled polymers [48] is largely due to the use of the phase matched transmission geometry which allows for greater interaction lengths. In practice, our sensitivity is ~100 lower and is believed to be due to excess laser noise. Modulation of the pump beam at significantly higher frequencies should reduce this noise. With the use of electro-optic materials exhibiting lower dispersion in the FIR, it should be possible to extend the bandwidth capability of this system with enhanced detection sensitivity.

VI. Optoelectronic Detection of Transient Electric Fields in High-Speed Circuits

The rapid progress in high speed electronic devices has created the demand for new measurement technologies. For maximum utility, these techniques must exhibit wide bandwidth, accurate signal reproduction, and minimal loading. In response to this need, several ultrafast optoelectronic methodologies including photoconductive sampling, electro-optic sampling, photoemissive sampling , and charge-sheet probing have been devised [57]. Electro-optic sampling

has received particular attention since it is capable of providing picosecond temporal resolution and submillivolt sensitivity [46]. In the case of GaAs, the electro-optic properties of the substrate itself may be exploited to perform *in-situ* measurements [58]. However, since the dominant electronic material, silicon, does not exhibit a linear electro-optic effect, an external probe is necessary.

A. High-Speed Electrical Sampling Using Optical Second-Harmonic Generation:-

Optical second harmonic generation (SHG) has been shown to be an effective tool for studying surfaces of centrosymmetric media [59, 60]. A high degree of sensitivity to electric fields has been demonstrated in studies of semiconductors, both with fields applied normal to the surface and under the influence of naturally occurring depletion fields [61-63]. Recently, Lupke *et al.* characterized the in-plane electric-field dependence in silicon using a transmission line structure [64]. These investigations suggest the possibility of measuring *transient* electric fields in high speed silicon-based devices. We have recently demonstrated the first measurement an ultrafast electrical pulse propagating on a transmission line with subpicosecond time resolution by SHG [65]. Since the method exploits the nonlinear optical response of silicon itself, it requires no additional probes or crystals and is non-invasive. In this approach, we expect the time resolution to be limited only by the laser pulse duration down to an inherent response time of less than 10 fs, while the spatial resolution is limited only by the focusing of the probe beam. Furthermore, the present scheme is readily applicable to silicon-based circuits without the need for any external probes and can, therefore, be used to examine high density integrated circuits.

We fabricated a coplanar waveguide transmission line on silicon-on-sapphire that was subsequently ion implanted. In addition to reducing the carrier lifetime to ~0.6 ps, we have found experimentally that this O^+ ion implantation step significantly improves the ohmic nature of the contacts, as demonstrated by the I-V characteristics. We used a 76 MHz mode-locked Ti:sapphire laser operating at 800 nm with 150 fs pulses as the optical source. A portion of the laser output served to launch picosecond electrical pulses onto the transmission line at a biased photoconductive gap. The electrical pulses were sampled at a nearby point between the coplanar lines by an s-polarized probe beam introduced with a variable temporal delay. For the SHG measurement, the s-polarized reflection was detected after passing through a series of filters using a photon counter, since this configuration suppressed the background signal. The s-polarized SH intensity, $I_s^{(2\omega)}$, may be related to the DC field, E_s^{dc}, oriented along the $\vec{s}$ direction by [60]

$$I_s^{(2\omega)} \propto \left|\chi_{sss}^{(2)} + \chi_{ssss}^{(3)} E_s^{dc}\right|^2 \left(I_s^{(\omega)}\right)^2, \qquad (21)$$

where ω is the frequency of the fundamental probe beam and $\chi^{(2)}$ and $\chi^{(3)}$ are the second order and third order susceptibilities, respectively.

First, we determined the dependence of the SH intensity on a static electric field produced by applying a DC bias to the transmission line and observed a parabolic dependence on the applied

voltage, as shown in fig. 31. The background contribution from $\chi^{(2)}$ is seen to be negligible, as anticipated for ion implanted silicon.

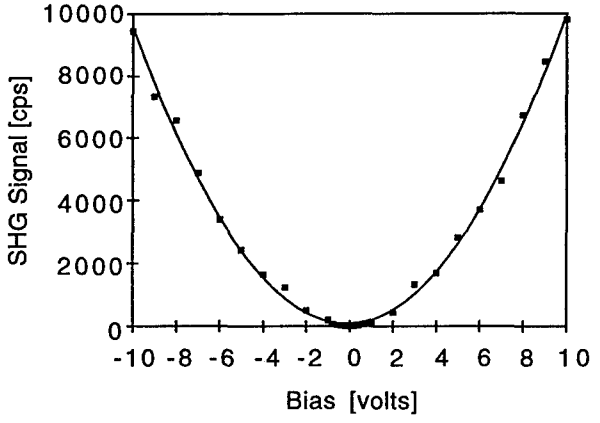

Figure 31

We then measured the transient electric field by placing a bias on the pump finger and gating the corresponding photoconductive gap. The time-resolved SH intensity $I_s^{(2\omega)}$, with and without an applied bias, is shown in fig. 32. We estimate that the peak pulse amplitude corresponds to a maximum voltage of 500 mV. The top waveform in this figure has a time response (FWHM) of approximately 1 ps. As expected, the SHG derived pulsewidth is comparable, but somewhat smaller, than the electronic cross-correlation pulsewidth of 1.55 ps derived from two photoconductive gaps.

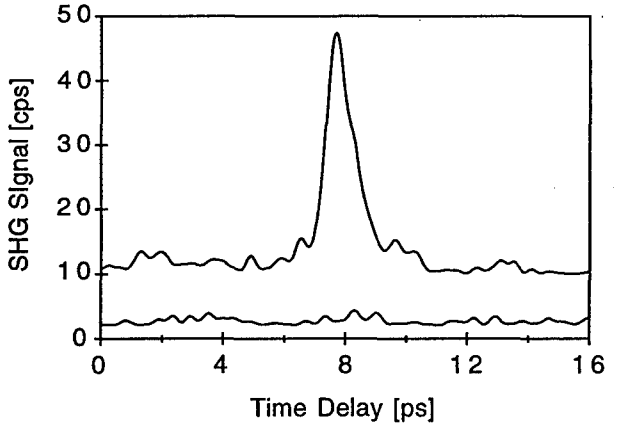

Figure 32

Electrical pulses propagating on such coplanar transmission lines have been characterized with subpicosecond time resolution and 100 mV/$\sqrt{\text{Hz}}$ sensitivity. Given the short escape depth (125 nm) for the SH signal and the expected electronic nature of the nonlinearity, an intrinsic response time of < 10 fs may be expected. A substantial improvement in the signal to noise ratio may be expected by using a photon energy for the probe lying below the band gap of Si. In this case, the technique would remain non-perturbative even for higher probe intensities, since no

carriers will be produced by the probe. Since the observed SH signal will still originate from the surface region of the silicon, the escape depth for the SH radiation (which lies above the band gap) will remain short. Furthermore, significantly tighter focusing of the incident probe beam, coupled with a reduction in the optical pulse duration, will yield a substantial enhancement in the sensitivity.

VII. Interactions and Technology Transfer

During the course of the research described in this report, the Columbia group has had several fruitful interactions and collaborations with industrial research organizations, government research facilities and academic institutions, as we discuss below.

A. Industrial interactions:-

The Ultrafast Optoelectronics Group at Columbia has had several interactions with various researchers at AT&T Bell Laboratories. The ion-implanted Si-on-sapphire dipole detectors used for our coherent THz measurements were fabricated with the assistance of Dr. Peter Smith at AT&T Bell Labs, Holmdel, New Jersey. The initial work on using large-aperture Si p-i-n diodes as THz emitters was done on samples provided by Dr. Bahram Jalali's group at AT&T Bell Labs, Murray Hill, New Jersey.

The Columbia group has collaborated extensively with Dr. James T. Yardley's organization at the AlliedSignal Technology Center in Morristown, New Jersey. This collaboration has allowed students at Columbia to have full access to materials, processing capabilities, and technical expertise related to poled polymers. In return, this interaction has yielded valuable information to AlliedSignal regarding the nonlinear optical properties of their materials.

The Columbia group has also interacted strongly with IBM T. J. Watson Research Center in Yorktown Heights, New York. In response to an interest in non-invasive high-speed probes of circuits, joint work was initiated with Dr. James A. Misewich of IBM Yorktown Heights. These investigations led to the formulation and demonstration of the SHG technique for the detection of ultrafast electrical transients that is described in the previous section of this report. Facilities at IBM Yorktown Heights have been made available for fabrication of custom optoelectronic devices required for these and other related investigations. Columbia group members have had access to IBM facilities and, conversely, IBM staff members have been involved in ultrafast optoelectronic measurements carried out at Columbia.

B. Interactions with DoD labs and other institutions:-

The Columbia group has collaborated extensively with Dr. Jeffrey D. Morse of Lawrence Livermore National Labs on various projects involving THz emission from photoconducting devices. Dr. Morse's group has provided various custom-fabricated semiconductor samples such as low-temperature MBE grown GaAs and GaAs p-i-n diodes.

With regards to detailed analyses and comprehensive modeling of THz emission from bulk semiconductors, we have worked closely with Dr. A.V. Kuznetsov and Prof. C.J. Stanton from the Department of Physics at the University of Florida at Gainesville. Our group has also interacted with Dr. L. A. Schlie at Phillips Labs in Kirtland Air Force Base, and has performed several measurements using available femtosecond laser capabilities to characterize the operation of high-speed THz detectors fabricated at Phillips Labs.

VIII. References

[1] W.M. Robertson, *Optoelectronic Techniques for Microwave and Millimeter-wave Engineering*, Boston: Artech House, 1995.

[2] D.H. Auston, "Ultrafast Optoelectronics," in *Ultrashort Laser Pulses*, 2nd edition, W. Kaiser, Ed., chapter 5, New York: Springer Verlag, 1993 and references therein.

[3] D. Grischkowsky in *Frontiers in Nonlinear Optics*, H. Walther, N. Koroteev, and M.O. Scully, Eds., Institute of Physics, Philadelphia, 1993.

[4] B.B. Hu and M.C. Nuss, Opt. Lett. **20**, 1716 (1995); Q. Wu, F.G. Sun, P. Campbell, and X.-C. Zhang, Appl. Phys. Lett. **68**, 3224 (1996).

[5] X.-C. Zhang, B.B. Hu, J.T. Darrow, and D.H. Auston, Appl. Phys. Lett. **56**, 1011 (1990).

[6] C. Jacoboni and L. Reggiani, Rev. Mod. Phys. **55**, 698 (1983).

[7] L. Xu, X.-C. Zhang, D. H. Auston, and B Jalali, Appl. Phys. Lett. **59**, 3357 (1991).

[8] L. Reggiani R. Brunetti, and C. Jacoboni, in Proceedings of the 3rd International Conference on Hot carriers in Semiconductors, J. Phys. Colloq. (Paris) **42**, C7-357 (1981).

[9] Ch. Fattinger and D. Grischkowsky, Appl. Phys. Lett. **54**, 490 (1989).

[10] J. Darrow, X.-C. Zhang, and D.H. Auston, Appl. Phys. Lett. **58**, 25 (1991).

[11] M. Yamanishi, Phys. Rev. Lett. **59**, 1014 (1987).

[12] D.A.B. Miller, and S. Schmitt-Rink, Phys. Rev. Lett. **59**, 1018 (1987).

[13] E. Yablonovitch, J.P. Heritage, D.E. Aspnes, and Y. Yafet, Phys. Rev. Lett. **63**, 976 (1989); Y. Yafet, E. Yablonovitch, Phys. Rev. B **43,** 12480 (1991).

[14] B. B. Hu, X.-C. Zhang and D. H. Auston, Phys. Rev. Lett. **67**, 2709 (1991).

[15] J.S. Blakemore, J. Appl. Phys **10**, . 53 (1982), and references therein.

[16] G.M. Wysin, D.L. Smith, and A. Redondo, Phys. Rev. B **38**, 12514, (1988).

[17] R. B. Hammond, Physica B+C **134B,** 475 (1985); M. C. Nuss, D. H. Auston, and F. Capasso, Phys. Rev. Lett. **58**, 2355 (1987); K. Meyer, M. Pessot, G. Mourou, R. Grondin, and S. Chamoun, Appl. Phys. Lett. **53**, 2254 (1988).

[18] A. E. Iverson, G. M. Wysin, D. L. Smith, and A. Redondo, Appl. Phys. Lett. **52**, 2148 (1988).

[19] S. L. Chuang, S. Schmitt-Rink, B. I. Greene, P. N. Saeta, and A. F. J. Levi, Phys. Rev. Lett. **68**, 102 (1992); B. I. Greene, J. F. Federici, D. R. Dykaar A. F. J. Levi, and L. Pfeiffer, Opt. Lett. **16**, 48 (1991).

[20] X.-C. Zhang, Y. Jin, K. Yang, and L. J. Schowalter, Phys. Rev. Lett. **69**, 2303 (1992); X.-C. Zhang, Y. Jin, K. Ware, X.F. Ma, A. Rice, D. Bliss, J. Larkin, and M. Alexander, Appl. Phys. Lett. **64**, 622 (1994); A. Rice, Y. Jin, X.F. Ma, X.-C. Zhang, D. Bliss, J. Larkin, and M. Alexander, Appl. Phys. Lett. **64**, 1324 (1994).

[21] P. C. Planken, M. C. Nuss, W. H. Knox, and D. A. B. Miller, Appl. Phys. Lett. **61**, 2009 (1992).

[22] B.B. Hu, L. Xu, J. T. Darrow, X.-C. Zhang, and D.H. Auston, in Dig. Quantum Electronics and Laser Science Conference, Opt. Soc. Amer., Washington, DC, (1992) JFA2.

[23] P. R. Smith, D. H. Auston, and M. C. Nuss, IEEE J. Quantum Electron. **24**, 255 (1988).

[24] Ch. Fattinger and D. Grischkowsky, Appl. Phys. Lett. **53**, 1480, (1988); Ch. Fattinger and D. Grischkowsky, Appl. Phys. Lett. **54**, 490, (1989).

[25] L. Xu, B. B. Hu, W. Xin, D. H. Auston, and J. Morse, Appl. Phys. Lett. **62**, 3507 (1993).

[26] A. V. Kuznetsov and C. J. Stanton, Phys. Rev. B **48**, 10828 (1993).

[27] S.M Sze, *Physics of Semiconductor Devices*, Wiley, New York, 1981.

[28] Y.R. Shen, Prog. Quantum Electron. **4**, 207 (1976).

[29] A.S. Weling, B.B. Hu, N.M. Froberg, and D.H. Auston, Appl. Phys. Lett. **64**, 137 (1994).

[30] E.B. Treacy, IEEE J. Quantum Electron. **QE-5**, 454 (1969).

[31] I.P. Christov and I.V. Tomov, Opt. Commun. **58**, 338 (1986).

[32] E.P. Ippen and C.V. Shank, in *Ultrashort Light Pulses*, S.L. Shapiro, Ed., Springer-Verlag, New York, 1977.

[33] P.K. Benicewicz, J.P. Roberts, and A.J. Taylor, J. Opt. Soc. Am. B **11**, 2533 (1994).

[34] C.H. Brito Cruz, P.C. Becker, R.L. Fork, and C.V. Shank, Opt. Lett. **13**, 123 (1988).

[35] J.T. Darrow, X.-C. Zhang, D.H. Auston, and J.D. Morse, IEEE J. Quantum Electron. **28**, 1607 (1992).

[36] G. Rodriguez, S.R. Caceres, and A.J. Taylor, Opt. Lett. **19**, 1994 (1994).

[37] J.R. Morris and Y. R. Shen, Optics Commun. **3**, 81 (1971).

[38] T. Yajima and N. Takeuchi, Jap. J. App. Phys. **10**, 907 (1971).

[39] P.R. Smith, D.H. Auston, and M.C. Nuss, IEEE J. Quantum Electron. **24**, 255 (1988).

[40] B.B. Hu, X.-C. Zhang, D.H. Auston, and P.R. Smith, Appl. Phys. Lett., **56**, 506 (1990).

[41] L. Xu, X.-C. Zhang, and D.H. Auston, Appl. Phys. Lett., **61**, 1784 (1992).

[42] X.F. Ma and X.-C. Zhang, J. Opt. Soc. Am. B, **10**, 1175 (1993); X.-C. Zhang, X.F. Ma, Y. Jin, T.-M. Liu, E.P. Boden, P.D. Phelps, K.R. Stewart, and C.P. Yakymyshyn, Appl. Phys. Lett. **61**, 3080 (1992); X.-C. Zhang, Y. Jin, and X.F. Ma, Appl. Phys. Lett. **61**, 2764 (1992).

[43] A. Nahata, J. Shan, J.T. Yardley, and C. Wu, J. Opt. Soc. Am. B, **10**, 1553 (1993).
[44] A. Nahata, D.H. Auston, C. Wu, and J.T. Yardley, Appl. Phys. Lett. **67**, 1358 (1995).
[45] K.D. Singer, M.G. Kuzyk, and J.E. Sohn, J. Opt. Soc. Am. B, **4**, 968 (1987).
[46] J.A. Valdmanis, G.A. Mourou, and C.W. Gabel, Appl. Phys. Lett. **41**, 211 (1982).
[47] A. Nahata, K.A. Horn, and J.T. Yardley, unpublished.
[48] A. Nahata, D.H. Auston, T.F. Heinz, and C. Wu, Appl. Phys. Lett. **68**, 150 (1996).
[49] Q. Wu and X.-C. Zhang, Appl. Phys. Lett. **67**, 3523 (1995); Q. Wu and X.-C. Zhang, Appl. Phys. Lett. **68**, 1604 (1996).
[50] D.H. Auston, K.P. Cheung, and P.R. Smith, Appl. Phys. Lett. **45**, 284 (1984).
[51] C.J. Bouwkamp, Rep. Prog. Phys. **17**, 35 (1954).
[52] D.H. Auston and M.C. Nuss, IEEE J. Quant. Electron. **24**, 184 (1988).
[53] A. Nahata , A.S. Weling, and T.F. Heinz, Appl. Phys. Lett. (submitted).
[54] Q. Wu, M. Litz and X.-C. Zhang, Appl. Phys. Lett. **68**, 2924 (1996).
[55] D.T.F. Marple, J. Appl. Phys. **25**, 539 (1964).
[56] T. Hattori, Y. Homma, A. Mitsuishi, and M. Tacke, Opt. Comm. **7**, 229 (1973).
[57] see for example, *Measurement of High-Speed Signals in Solid State Devices (Semiconductors and Semimetals, vol. 28)*, R.B. Marcus, ed. (Academic, Boston, 1990).
[58] B.H. Kolner and D.M. Bloom, IEEE J. Quant. Electron. **QE-22**, 79 (1986).
[59] Y.R. Shen, Nature **337**, 519 (1989).
[60] T.F. Heinz, in *Nonlinear Surface Electromagnetic Phenomena*, ed. by H.-E. Ponath and G. Stegeman, 353 (Elsevier, Amsterdam, 1991); G. A. Reider and T. F. Heinz, in *Photonic Probes of Surfaces: Electromagnetic Waves*, vol. 2, ed. by P. Halevi, (Elsevier, Amsterdam, 1995).
[61] C.H. Lee, R.K. Chang, and N. Bloembergen, Phys. Rev. Lett. **18**, 167 (1967).
[62] J. Qi, M.S. Yeganeh, I. Koltover, A.G. Yodh, and W.M. Theis, Phys. Rev. Lett. **71**, 633 (1993).
[63] J.G. Mihaychuk, J. Bloch, Y. Liu, and H.M. van Driel, Opt. Lett. **20**, 2063 (1995).
[64] G. Lupke, C. Meyer, C. Ohloff, H. Kurz, S. Lehmann, and G. Marowsky, Opt. Lett. **20**, 1997 (1995).
[65] A. Nahata, T.F. Heinz, and J.A. Misewich, Appl. Phys. Lett. (in press).

IX. Publications

1. A. Nahata , A.S. Weling, and T.F. Heinz, "A Wideband Coherent Terahertz Spectroscopy System Using Optical Rectification and Electro-optic Sampling," Appl. Phys. Lett. (submitted).
2. A. Nahata, T.F. Heinz, and J.A. Misewich, "High Speed Electrical Sampling Using Optical Second Harmonic Generation," Appl. Phys. Lett. (in press).
3. A.S. Weling and D.H. Auston, "Novel Sources and Detectors for Coherent Tunable Narrowband Terahertz Radiation in Free Space," J. Opt. Soc. Am. B (in press).
4. A. Nahata, D.H. Auston, T.F. Heinz, and C. Wu, "Coherent Detection of Freely Propagating Terahertz Radiation by Electro-optic Sampling in a Poled Polymer," Appl. Phys. Lett. **68**, 150 (1996).
5. A. Nahata, D.H. Auston, C. Wu, and J.T. Yardley, "Generation of Terahertz Radiation From a Poled Polymer," Appl. Phys. Lett. **67**, 1358 (1995).
6. A.S. Weling, B.B. Hu, N.M. Froberg, and D.H. Auston, "Generation of Tunable Narrow Band THz Radiation from Large Aperture Photoconducting Antennas," App. Phys. Lett. **64**, 137 (1994).
7. B.B. Hu, A.S. Weling, D.H. Auston, A.V. Kuznetsov, and C.J. Stanton, "DC-Electric Field Dependence of THz Radiation Induced by Femtosecond Optical Excitation of Bulk GaAs," Phys. Rev. B **49**, 2234 (1994).
8. L. Xu, B.B. Hu, W. Xin, D.H. Auston, and J. D. Morse, "Hot Electron Dynamics Study by Terahertz Radiation from Large Aperture GaAs *p-i-n* Diodes," Appl. Phys. Lett. **62**, 3507 (1993).
9. L. Xu, X.C. Zhang, and D. H. Auston, "Terahertz Beam Generation by Femtosecond Optical Pulses from ELectro-optic Materials," Appl. Phys. Lett. **61**, 1784 (1993).
10. N. M. Froberg, B. B. Hu, X.-C. Zhang, and D. H. Auston, "Terahertz Radiation from a Photoconducting Antenna Array," IEEE J. of Quantum Electron. **28**, 2291 (1992).
11. J. T. Darrow, X.-C. Zhang, D.H. Auston, and J. D. Morse, "Saturation Properties Of Large-Aperture Photoconducting Antennas," IEEE J. Quantum Electron. **28**, 1607 (1992).
12. L. Xu, D.H. Auston, and A. Hasegawa, "Propagation of Electromagnetic Solitary Waves in Dispersive Nonlinear Dielectrics," Phys. Rev. A **45**, 3184 (1992).
13. X.-C. Zhang and D. H. Auston, "Optoelectronic measurement of semiconductor surfaces and interface with femtosecond optics," J. Appl. Phys. **71**, 326 (1992).
14. B.B. Hu, X.-C Zhang and D.H. Auston, "Terahertz Radiation Induced by Sub-Bandgap Femtosecond Optical Excitation," Phys. Rev. Lett. **67**, 2709 (1991).
15. L. Xu, X.-C. Zhang, D. H. Auston and B. Jalali, "Terahertz radiation from large aperture Si p-i-n diode," Appl. Phys. Lett. **59**, 3357 (1991).
16. L. Xu, X.-C. Zhang, D.H. Auston, and W.I. Wang, "Internal Piezoelectric Field in Strained Layer GaInSb/InAs Superlattices Probed by Optically Induced Microwave Radiation," Appl. Phys. Lett. **59**, 3562 (1991).
17. N. M. Froberg, B. B. Hu, X.-C. Zhang, and D. H. Auston, "Time-division Multiplexing by a Photoconducting Antenna Array," Appl. Phys. Lett. **59**, 3207 (1991).
18. X.-C. Zhang and D.H. Auston, "Generation of Steerable Submillimeter-Waves from Semiconductor Surfaces by Spatial Light Modulators," Appl. Phys. Lett., **59**, 768 (1991).

X. Presentations

1. A. Nahata, T.F. Heinz, and J.A. Misewich, "High speed circuit testing using optical second harmonic generation," presented at *CLEO* (OSA, Anaheim, CA), 1996.
2. A. Nahata, T.F. Heinz, and J.A. Misewich, "High speed circuit testing using optical second harmonic generation," presented at *Ultrafast Phenomena X*, (OSA, San Diego, CA), 1996.
3. A.S. Weling, D.H. Auston, and T.F. Heinz, "Tunable photoconducting emitters and detectors of free space terahertz radiation," presented at *Ultrafast Phenomena X*, (OSA, San Diego, CA), 1996.
4. A. Nahata, T.F. Heinz, and J.A. Misewich, "Ultrafast measurement of electric fields in semiconductors by optical second-harmonic generation," Bull. Am. Phys. Soc. (Annual Meeting, St. Louis, MO), 1996.
5. A.S. Weling, T.F. Heinz, and D.H. Auston, "Saturation effects in narrowband terahertz generation by chirped pulse mixing in biased photoconductors," Bull. Am. Phys. Soc. (Annual Meeting, St. Louis, MO), 1996.
6. A. Nahata, T.F. Heinz, D.H. Auston, and C. Wu, "Coherent detection of freely propagating terahertz radiation by electro-optic sampling in a poled polymer," presented as a post-deadline paper at *Organic Thin Films Conference for Photonic Applications* (OSA Technical Digest, vol. 21), 1995.
7. A. Nahata, C. Wu, J.T. Yardley, and D.H. Auston, "Generation of terahertz radiation from an organic poled polymer," presented as a post-deadline paper at *QELS* (OSA, Baltimore, MD), 1995.
8. A. Nahata, C. Wu, J.T. Yardley, and D.H. Auston, "Generation of terahertz radiation from a poled polymer," presented as a post-deadline paper *Ultrafast Electronics and Optoelectronics Conference* (OSA, Dana Point, CA), 1995.
9. A.S. Weling, B.B. Hu, N.M. Froberg, and D.H. Auston, "Generation of tunable narrow band THz radiation from large aperture photoconducting antennas," presented at *CLEO* (OSA, Anaheim, CA), 1994.
10. A.S. Weling, B.B. Hu, N.M. Froberg, and D.H. Auston, "Generation of tunable narrow band free space THz radiation," in *Ultrafast Phenomena IX*, P.F. Barbara et al. eds., Springer Series in Chem. Phys., vol. 60, 405 (1994).
11. B.B. Hu, A.S. Weling, D.H. Auston, and A.V. Kuznetsov, "dc-Electric field dependence of THz radiation induced by femtosecond optical excitation of bulk GaAs," presented as a post-deadline paper at *QELS* (OSA, Baltimore, MD), 1993.
12. B.B. Hu, L. Xu, and D. H. Auston, "Generation of THz radiation from semiconductor optoelectronics devices," invited talk at the *IEEE/LEOS Summer Topical Meeting* (IEEE, Santa Barbara, CA), 1993.
13. B. B. Hu and D. H. Auston, " THz radiation from photoconducting antenna," invited talk at the *IEEE/MTT Workshop on Picosecond and Femtosecond Electromagnetic Pulses* (IEEE, Atlanta, GA), 1993.
14. B.B. Hu, L. Xu, J. T. Darrow, X.-C. Zhang, and D.H. Auston, "Terahertz radiation from semiconductor surfaces" presented as an invited paper at *QELS*, (OSA Technical Digest, Washington, DC), 1992.
15. L. Xu, B.B. Hu, X.-C. Zhang and D. H. Auston, "Generation of femtosecond radiation from photovoltaic devices," in the *Proceedings of the Twenty Second IEEE Photovoltaic Specialists Conference*, 329 (1991).

16. B.B. Hu, X.-C. Zhang, and D.H. Auston, "Observation of negative photoconductivity in GaAs," presented as a postdeadline paper at *QELS*, (OSA Technical Digest, Washington, DC), 1991.

17. D. H. Auston and X.-C. Zhang, "Large-Aperture photoconducting antennas," in the *OSA Proceedings on Picosecond Electronics and Optoelectronics*, T.C.L.G. Sollner and J. Shah (eds.), vol. 9, 2 (1991).

XI. Personnel

The following personnel have been associated with the research conducted under this grant at Columbia:

1. Prof. Tony F. Heinz (1995-96), Professor of Electrical Engineering and Physics
2. Prof. David H. Auston* (1991-94), Professor of Electrical Engineering and Applied Physics and Dean of the School of Engineering and Applied Sciences
3. Prof. X.-C. Zhang** (1991), Research Scientist
4. Dr. Binbin Hu (1992-93), Post-doctoral Research Scientist
5. Graduate Students: Binbin Hu, Li Xu, Aniruddha Weling, Ajay Nahata, and Julie Soltz

* Present address: Office of the Provost, Rice University, 206 Lovett Hall, 6100 S. Main Street, Houston TX 77005.

** Present address: Department of Physics, Rensselaer Polytechnic Institute, Troy NY 12180-3590